การสังเคราะห์โครงสร้างระดับนาโนเมตรของทองคำที่ซับซ้อนโดยเหนี่ยวนำด้วยไอออนเงิน

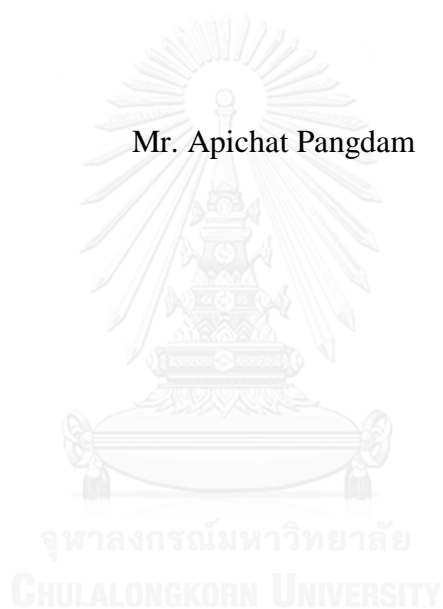นายอภิชาติ เพ็งดำ

วิทยานิพนธ์นี้เป็นส่วนหนึ่งของการศึกษาตามหลักสูตรปริญญาวิทยาศาสตรดุษฎีบัณฑิต
สาขาวิชาเคมี ภาควิชาเคมี
คณะวิทยาศาสตร์ จุฬาลงกรณ์มหาวิทยาลัย
ปีการศึกษา 2559
ลิขสิทธิ์ของจุฬาลงกรณ์มหาวิทยาลัย

SYNTHESIS OF COMPLEX GOLD NANOSTRUCTURES INDUCED
BY SILVER ION

Mr. Apichat Pangdam

A Dissertation Submitted in Partial Fulfillment of the Requirements
for the Degree of Doctor of Philosophy Program in Chemistry
Department of Chemistry
Faculty of Science
Chulalongkorn University
Academic Year 2016
Copyright of Chulalongkorn University

Thesis Title	SYNTHESIS OF COMPLEX GOLD NANOSTRUCTURES INDUCED BY SILVER ION
By	Mr. Apichat Pangdam
Field of Study	Chemistry
Thesis Advisor	Professor Sanong Ekgasit, Ph.D.
Thesis Co-Advisor	Associate Professor Chuchaat Thammacharoen

Accepted by the Faculty of Science, Chulalongkorn University in Partial Fulfillment of the Requirements for the Doctoral Degree

.... Dean of the Faculty of Science
(Associate Professor Polkit Sangvanich, Ph.D.)

THESIS COMMITTEE

.... Chairman
(Associate Professor Warinthorn Chavasiri, Ph.D.)

.... Thesis Advisor
(Professor Sanong Ekgasit, Ph.D.)

.... Thesis Co-Advisor
(Associate Professor Chuchaat Thammacharoen)

.... Examiner
(Assistant Professor Kanet Wongravee, Ph.D.)

.... Examiner
(Numpon Insin, Ph.D.)

.... Examiner
(Assistant Professor Boonrat Lohwongwatana, Ph.D.)

.... External Examiner
(Associate Professor Chinapong Kritayakornupong, Dr.rer.nat.)

อภิชาติ เพ็งดำ : การสังเคราะห์โครงสร้างระดับนาโนเมตรของทองคำที่ซับซ้อนโดยเหนี่ยวนำด้วยไอออนเงิน (SYNTHESIS OF COMPLEX GOLD NANOSTRUCTURES INDUCED BY SILVER ION) อ.ที่ปรึกษาวิทยานิพนธ์หลัก: ศ. ดร. สนอง เอกสิทธิ์, อ.ที่ปรึกษาวิทยานิพนธ์ร่วม: รศ. ชูชาติ ธรรมเจริญ, 81 หน้า.

ในงานวิจัยนี้ปฏิกิริยาที่มีความเฉพาะตัวของไอออนเงินถูกใช้ในการสังเคราะห์และการควบคุมความยาวของโครงสร้างระดับนาโนเมตรแบบหนาม ที่อยู่บนโครงสร้างทองคำระดับไมโครเมตรที่มีรูปร่างคล้ายหอยเม่น โครงสร้างที่ถูกพัฒนาขึ้นสามารถสังเคราะห์ได้ง่ายในขั้นตอนเดียวด้วยกระบวนการสังเคราะห์ที่ปราศจากการใช้สารปกป้องพื้นผิวและสารช่วยเสถียร สารเคมีที่ใช้ในการสังเคราะห์ประกอบด้วย เตตระคลอโรออริก (III) แอซิด ซิลเวอร์ไนเตรท และไฮโดรเจนเปอร์ออกไซด์ ซึ่งไฮโดรเจนเปอร์ออกไซด์ทำหน้าที่เป็นตัวรีดิวซ์เพียงสารเดียว ขณะที่ไอออนเงินที่ความเข้มข้นต่ำมากทำหน้าที่สำคัญในการควบคุมโครงสร้าง กรณีที่ไม่มีการเติมไอออนเงินในกระบวนการสังเคราะห์ โครงสร้างทองคำระดับไมโครเมตรคล้ายทรงกลมจะปรากฏขึ้น จากการศึกษาการเปลี่ยนแปลงของโครงสร้างเทียบกับเวลาที่ใช้ในการสังเคราะห์ด้วยกล้องจุลทรรศน์อิเล็กตรอนแบบส่องกราด พบว่าโครงสร้างทองคำระดับไมโครเมตรที่มีรูปร่างคล้ายหอยเม่น และโครงสร้างคล้ายทรงกลม มีความเกี่ยวข้องและพัฒนามาจากโครงสร้างเดียวกันคือโครงสร้างทองคำในระดับไมโครเมตรคล้ายดอกไม้ โดยไอออนเงินที่ถูกเติมเข้าไปในกระบวนการสังเคราะห์สามารถเกิดการดูดซับทางกายภาพบนผิวของทองคำและเปลี่ยนเป็นซิลเวอร์คลอไรด์ในรูปของแข็งที่มีความสามารถในการยับยั้งการโตแบบเดนไดรต์ ส่งผลให้โครงสร้างหนามที่ยื่นออกมาพัฒนาเป็นโครงสร้างที่มีรูปร่างคล้ายหอยเม่น โครงสร้างที่ถูกพัฒนาในข้างต้นมีพื้นผิวที่สะอาด ให้สัญญาณรามานที่สูงเมื่อใช้เป็นวัสดุรองรับในเทคนิคพื้นผิวขยายสัญญาณรามาน พบว่าความยาวเฉลี่ยของโครงสร้างระดับนาโนเมตรแบบหนาม คือ 166 และ 187 นาโนเมตร สามารถช่วยเพิ่มสัญญาณรามานในการตรวจวิเคราะห์สาร โรตามีน 6จี ความเข้มข้น 0.1 นาโนโมลาร์ ในระยะเวลาการเตรียมตัวอย่างที่สั้นคือ 15 นาที นอกจากนี้ โครงสร้างทองคำระดับไมโครเมตรที่มีลักษณะคล้ายหอยเม่น สามารถค้นหาตำแหน่งของตัวอย่างที่สนใจได้ง่ายภายใต้กล้องจุลทรรศน์ ช่วยในการพิสูจน์เอกลักษณ์ทางเคมีได้ทันทีด้วยเทคนิคพื้นผิวขยายสัญญาณรามาน

ภาควิชา	เคมี	ลายมือชื่อนิสิต	....
สาขาวิชา	เคมี	ลายมือชื่อ อ.ที่ปรึกษาหลัก	....
ปีการศึกษา	2559	ลายมือชื่อ อ.ที่ปรึกษาร่วม	....

v

5273869723 : MAJOR CHEMISTRY

KEYWORDS: SILVER IONS / DENDRITIC GROWTH / SERS / LSPR / URCHIN-LIKE GOLD MICROSTRUCTURES

APICHAT PANGDAM: SYNTHESIS OF COMPLEX GOLD NANOSTRUCTURES INDUCED BY SILVER ION. ADVISOR: PROF. SANONG EKGASIT, Ph.D., CO-ADVISOR: ASSOC. PROF. CHUCHAAT THAMMACHAROEN, 81 pp.

In this work, we exploited a unique reaction of silver ions to create and design urchin-like gold microstructures (UL-AuMSs) with controllable length of nanothorns. The UL-AuMSs were synthesized via a simple one-pot synthetic protocol without using any surface capping agents or polymeric stabilizers. The reactants consisted of tetrachloroauric (III) acid, silver nitrate, and hydrogen peroxide (H_2O_2). H_2O_2 functioned as the sole reducing agent while trace silver ions played an important role as the shape controlling agent. Without trace silver ions, quasi-sphere gold microstructures (QS-AuMSs) were obtained. The time-dependent SEM investigations corroborated that UL-AuMSs and QS-AuMSs grew from flower-like gold microstructures (FL-AuMSs). The added trace silver ions reacted with physically adsorbed chloride ions on gold surfaces and formed into solid silver chloride capable of altering the dendritic growth of QS-AuMSs to the dominated trunk-growth of UL-AuMSs. The cleaned UL-AuMSs with average thorn lengths of 166 and 187 nm expressed high SERS activity as 0.1 nM of Rhodamine 6G could be detected with a short 15-min incubation. The easily visualized UL-AuMSs under a microscope assisting the SERS detection at selected spots was demonstrated.

Department:	Chemistry	Student's Signature
Field of Study:	Chemistry	Advisor's Signature
Academic Year:	2016	Co-Advisor's Signature

ACKNOWLEDGEMENTS

CONTENTS

LIST OF TABLES

จุฬาลงกรณ์มหาวิทยาลัย
CHULALONGKORN UNIVERSITY

LIST OF SCHEME

LIST OF FIGURES

Figure   Page

LIST OF SYMBOLS

ω_0 : Initial frequency

ω_R : Raman scattered frequency

E_{loc} : Local electric field

E_0 : Electric field form absent nanoparticles

$G_1(\omega_0)$: Enhancement factors from initial frequency

$G_2(\omega_R)$: Enhancement factors from Raman scattered frequency

LIST OF ABBREVIATIONS

EDX   : Energy-dispersive X-ray spectroscopy

SERS   : Surface enhanced Raman scattering

LSPR   : Localized surface plasmon resonance

SAED   : Selected area electron diffraction

SEI   : Secondary electron imaging

DLA   : Diffusion-limited aggregation

PEDOT: PSS   : Poly(3,4-ethylenedioxythiophene) polystyrene sulfonate

PAHs   : Polycyclic aromatic hydrocarbons

R6G   : Rhodamine 6G

RhB   : Rhodamine B

PATP   *: p*-aminothiophenol

CTAB   : Cetyltrimethylammonium bromide

SEM   : Scanning electron microscope

TEM   : Transmission electron microscope

HRTEM   : High-resolution transmission electron microscope

AuNPs   : Gold nanoparticles

QS-AuMSs   : Quasi-sphere gold microstructures

UL-AuMSs   : Urchin-like gold microstructures

FL-AuMSs   : Flower-like gold microstructures

HS-AuMSs   : Hemi-spherical gold microstructures

UL-AuNPs   : Urchin-like gold nanoparticles

CHAPTER I
INTRODUCTION

1.1   Research background and rationale

Multipod gold nanostructures such as dendritic gold nanoparticles, [1-3] gold nanostars, [4-6] and urchin-like gold nanoparticles [7-9] have gained considerable attention as their unique nano-enable properties could be tuned by the manipulations of the number, size, and length of the pods. [10] The branch structures have exceptionally strong electric field (hot spot) at the tips and gaps between pods. [11, 12] The multipod gold nanostructures were successfully employed as SERS substrates for trace analysis of p-aminothiophenol, [13] p-mercaptobenzoic acid [14] and lucigenin. [15] Several chemical-based synthetic approaches for generating multipod gold nanostructures were developed, including electrochemical, [16] galvanic replacement, [17] and seed-mediation. [17-21] The chemical processes have attracted great interests as they are versatile and effective. The complex gold microstructures were selectively produced using various reducing agents and stabilizers. The reducing agents such as hydroxylamine hydrochloride [17, 18, 21] and ascorbic acid [19, 20] were employed. The particle size and shape were controlled by capping agents or stabilizers. Several researchers employed silver ions (Ag^+) [17-21] and organic stabilizer (*i.e.,* cetyltrimethylammonium bromide (CTAB)) [19, 20] for multipod nanostructures fabrications.

In this study, we exploited the unique reaction of trace Ag^+ on designing urchin-like gold microstructures (UL-AuMSs) with controllable length of nanothorns. The organic capping agents or polymeric stabilizers were not employed in this work. We

also confirmed the governing mechanism of trace Ag^+ on the formation and growth of nanothorns. Hydrogen peroxide (H_2O_2) was employed as the sole reducing agent while trace Ag^+ was used as a shape-controlling agent. We took advantage of the selectively surface passivation of chloride ions (Cl^-) on gold surface for the formation of solid silver chloride (AgCl) when the trace Ag^+ was added. The adsorbed solid AgCl on gold surface altered the growth mechanism of the UL-AuMSs. Systematic time-dependent SEM investigations were performed in order to gain an insight understanding on the growth mechanism of the thorn structures. By changing the concentration of trace Ag^+, we could selectively tune the length of nanothorn. A potential application of UL-AuMSs as a powerful SERS substrate was explored.

1.2 Objectives

To develop synthesis protocol for complex gold microstructure with gold nanothorns using silver ions as the shape controlling agent.

1.3 Scope of the dissertation

1.3.1 Study the optimum condition for complex gold microstructure with gold nanothorns using silver ions as shape controlling agent.

1.3.2 Study the morphology of complex gold microstructure with gold nanothorns and explain the growth mechanism.

1.3.3 Demonstrate the application of complex gold microstructure with gold nanothorns as substrate for surface enhanced Raman substrate (SERS) for trace chemical analysis.

1.4   Benefits of the dissertation

1.4.1   Understanding of the growth mechanism of complex gold microstructure with gold nanothorns on the surface is necessary for structural synthesis control.

1.4.2   Using complex gold microstructure with gold nanothorns as surface enhanced Raman substrate (SERS) is widely applied for trace chemical analysis under Raman microscope.

CHAPTER II
THEORETICAL BACKGROUND

2.1 Nanoscience and Nanotechnology

Nanotechnology is the multidisciplinary researches covering science, engineering, and technology to control size and shape of material at the nanometer scale as shown in Figure 2-1. The novel properties of nanomaterials are different from their bulks material due to highly increasing of surface area and confinement of electrons. [22]
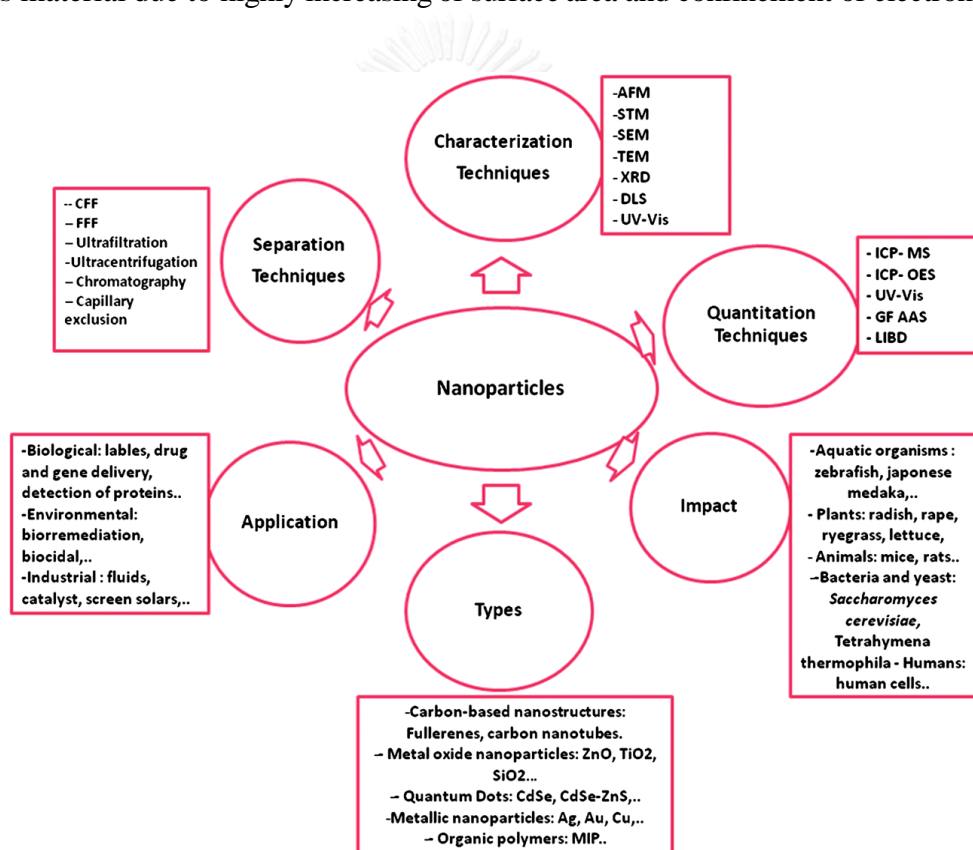
Figure 2-1 Multidisciplinary researches for nanoscience and nanotechnology. Reprinted (adapted) with permission from [22] Copyright (2013) Royal Society of Chemistry.

Via nanoscience and nanotechnology, the particle size of nanomaterials was controlled in the range of 1-100 nm in any dimension. Nanomaterials or nanoparticles had been emerged with unique physical and chemical properties which can be used in diverse applications in many areas such as chemistry, biology, physics, materials science, and engineering. [23]

2.2 Gold nanoparticles and applications

Gold nanoparticles (AuNPs) are one of the most studied nanomaterials due to their remarkable chemical and physical properties such as superior catalytic activity, [25, 26] electrical conductivity, [27, 28] surface functionality, [29, 30] and optical property. [31, 32] with exceptional stability under diverse environments [24] Especially, the optical property of AuNPs is widely applied to many research fields, which strongly depend on their size and shape, as shown in Figures 2-2 and 2-3. This could be explained by localized surface plasmon resonance (LSPR).
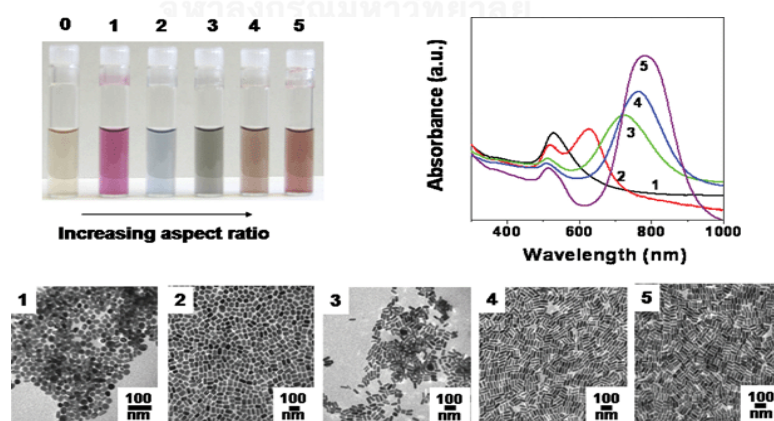
Figure 2-2   The UV-Vis spectra and TEM micrographs for (0) spherical gold nanoparticles and (1–5) gold nanorods at different aspect ratio. Reprinted (adapted) with permission from [33] Copyright (2007) Royal Society of Chemistry.
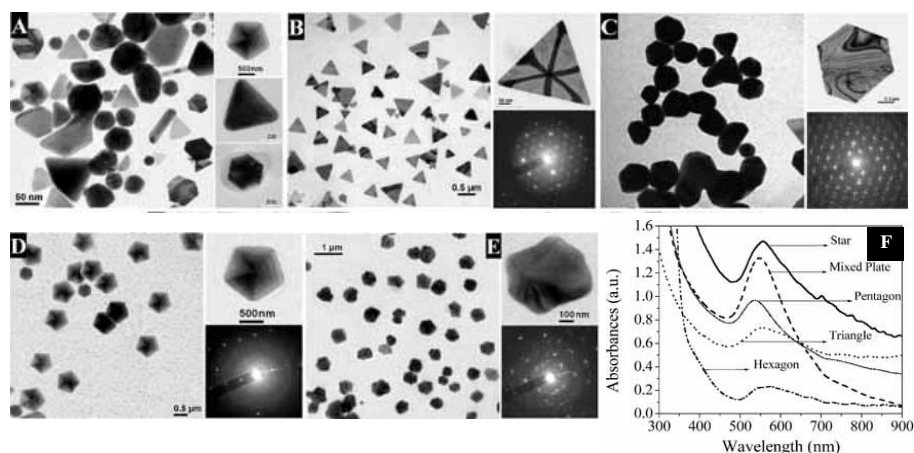
Figure 2-3   TEM images and SAED patterns (insert figures) of different shapes of gold nanoplates synthesized under different reaction conditions (A) mixed nanoplates, (B) triangle-, (C) hexagon-, (D) pentagon-, and (E) star-shaped gold nanoplates. (F) UV/Vis spectra of gold nanoplates. Reprinted (adapted) with permission from [34] Copyright (2010) John Wiley and Sons.

2.3   Localized surface plasmon resonance (LSPR)

The relation of metal nanoparticles and electromagnetic field enhancement were thoroughly explained by localized surface plasmon resonance (LSPR), as shown in Figure 2-4. When the particle size of metal is reduced to nanoscale, electron on the surface of metal nanoparticles is localized by quantum-size effect. [35] The group of electron on metal nanoparticle surface or electron cloud can oscillate or move in specific direction. The oscillation of electron cloud is called plasmon oscillation. When incident photon interacts with surface of metal nanoparticles with a similar frequency of plasmon oscillation, an electromagnetic field will be enhanced by resonance frequency between photon and plasmon.
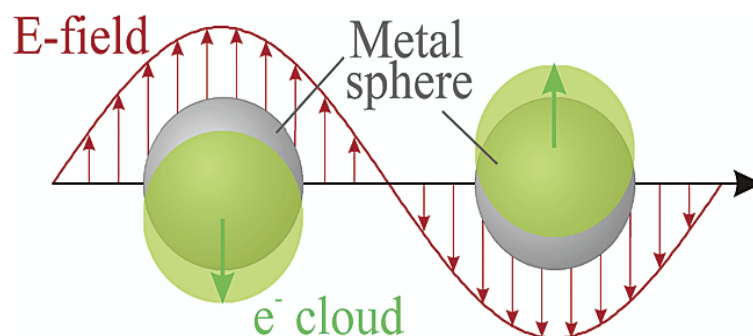
Figure 2-4   Schematic illustration of electron cloud oscillation generating localized surface plasmon resonance (LSPR) of metal nanospheres. Reprinted (adapted) with permission from [36] Copyright (2003) American Chemical Society.

This result can produce strong light absorption, high electric field enchantment and high thermal flux on metal nanoparticles which can be applied in color metric sensor, surface enhanced Raman scattering and thermal plasmonic. The plasmonic properties of AuNPs were widely used in many applications as shown in previous part due to precisely structural controllability, high durability in strong redox condition, ease of surface functionalization and optically tunable in visible region. The LSPR properties directly depend on morphology (particle size and shape) and surrounding medium. [36] Therefore, the basic knowledge of engineering nanostructure could be necessary for tuning plasmonic properties to meet the appropriated applications such as colorimetric hydration sensor for sport activities (Figure 2-5), [37] plasmonic heater in cancer therapy (Figure 2-6), [38] light trapping in solar cell (Figure 2-7), [39] and surface enhanced Raman scattering (SERS) substrate for selective detection of pollutants in real environments (Figure 2-8). [40]
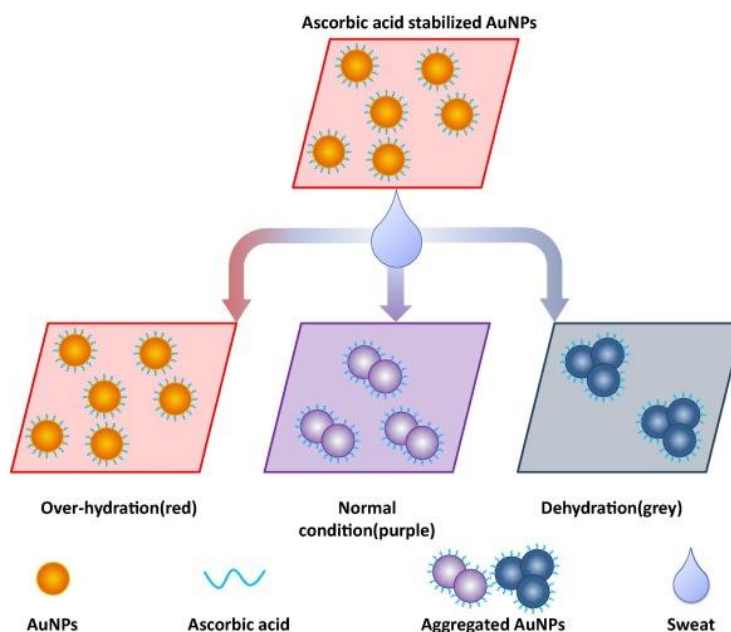
Figure 2-5 Schematic illustration of the colorimetric dehydration sensor on aggregation of gold nanoparticles for sport activities. Reprinted (adapted) with permission from [37] Copyright (2016) Elsevier.
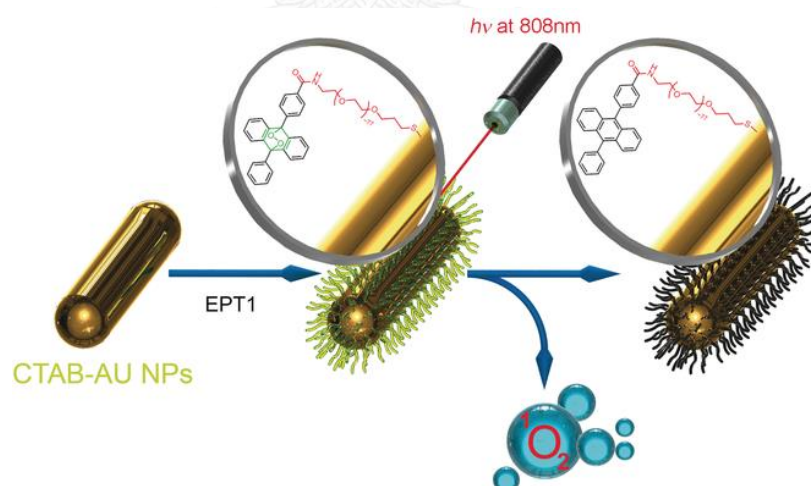
Figure 2-6 Schematic illustration of the gold nanorods at near-IR wavelengths leading to thermal cycloreversion of the tethered endoperoxides and yielding singlet oxygen for cancer therapy by plasmonic heating. Reprinted (adapted) with permission from [38] Copyright (2016) John Wiley and Sons.
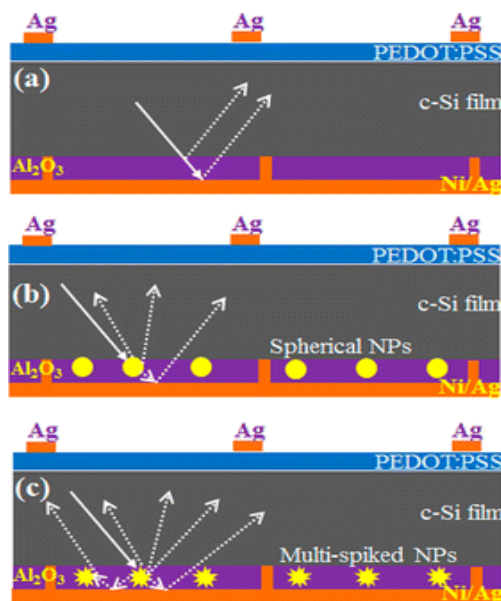
Figure 2-7   Schematic illustration of scattering patterns in ultrathin c-Si/PEDOT:PSS hybrid solar cell (a) without gold nanoparticles, (b) spherical and (c) multispiked nanoparticles. Reprinted (adapted) with permission from [39] Copyright (2014) American Chemical Society.
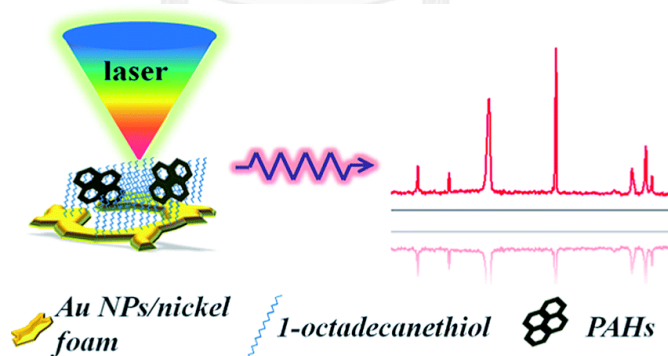
Figure 2-8   Schematic illustration for the fabrication process of the 3D gold nanoparticles (AuNPs)/nickel foam as SERS substrate and their application for selective detection of poly aromatic hydrocarbons (PAHs) in real environments. Reprinted (adapted) with permission from [40] Copyright (2015) Royal Society of Chemistry.

2.4   Surface enhanced Raman spectroscopy (SERS)

Raman spectroscopy was widely used for trace chemical analysis in environment, food safety, forensic and medical diagnosis. The potential of Raman spectroscopy for chemical detection in analytical chemistry is from micromolar to single molecules. However, the signal obtained from Raman scattering is weak~0.001% of the incident photons producing Raman scattering but approximately 99.999% of incident light as Rayleigh scattering. In order to increase Raman signal, surface enhanced Raman spectroscopy (SERS) was developed. Raman signal-enhanced process on metal substrate is activated by chemical and electromagnetic effect. The electromagnetic enhancement is the main parameter to give a large Raman signal enhancement of 10^{14} times comparing with unenhanced signal. The electromagnetic effect on SERS phenomenal could be explained by LSPR on metal nanoparticles employed as substrate in SERS technique, as shown Figure 2-9. [41]

There are two processes to enhance electromagnetic field in SERS. Firstly, the local electromagnetic field enhancement is generated around metal nanoparticles by the incident photon with initial frequency (ω_0). Plasmonic activity serves as receiving optical antennae to convert the far field (incident photon) to the near field on surface of metal nanoparticles. Subsequently, the Raman scattered frequency (ω_R) form adsorbed Raman active molecules on metal surface were enhanced by near field, which are typically one to three orders of magnitude larger than those of the free molecules. The enhancement power in this step is relative to the square of the local electric field (E_{loc}) at ω_R. [42]
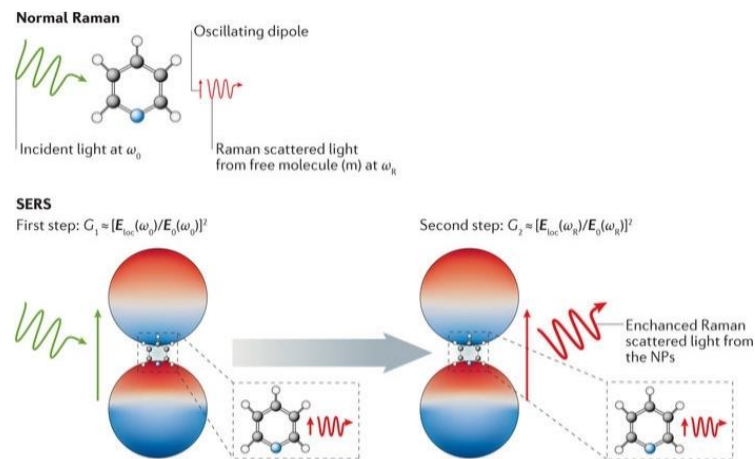
Figure 2-9   Principle of the surface enhanced Raman scattering. Reprinted (adapted) with permission from [42] Copyright (2016) Nature Publishing Group.

The enhancement factors of the first and second steps ($G_1(\omega_0)$ and $G_2(\omega_R)$, respectively) are approximately proportional to the fourth power of the enhancement of the local electric field (which E_{loc} and E_0 are the local electric fields in the presence and absence of nanoparticles, respectively), as shown in Eq. 2-1. [42]

$$G = G_1(\omega_0)G_2(\omega_R) = \frac{|E_{loc}(\omega_0)|^2|E_{loc}(\omega_R)|^2}{|E_0(\omega_0)|^2|E_0(\omega_R)|^2} \approx \frac{|E_{loc}(\omega_R)|^4}{|E_0(\omega_0)|^4} \qquad \text{(Eq. 2-1)}$$

2.5   Synthesis of AuNPs

The synthesis protocols of AuNPs could be separated into top-down and bottom-up process as shown in Figure 2-10. The top-down process is the method that diminish size or volume of bulk materials to nanoparticles. On the other hand, bottom-up processing is the method to accumulate atoms or molecules into nanoparticles. The particles size could be controlled by degree of diminishing or accumulating. [43]

Generally, the synthetic protocols of AuNPs can be done in physical and chemical approach, respectively. [44]
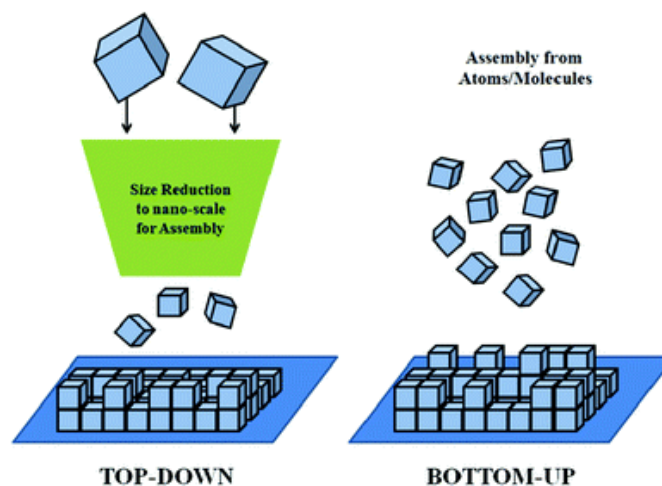
Figure 2-10 Top-down and bottom-up approaches in nanotechnology. Reprinted (adapted) with permission from [43] Copyright (2012) Royal Society of Chemistry.

2.5.1 Synthesis of AuNPs in physical approach

In this approach, the bulk gold metal will be decreased its size and formed gold AuNPs with difference size and shape by mechanical process for example; the electron-beam lithography that made gold nanostructures for surface-enhanced Raman substrate (SERS) (Figure 2-11), [45] the thermal evaporation technique that fabricated the ultrathin gold nanoparticles for light trapping in organic photosensitive diodes (Figure 2-12), [46] and the laser ablation technique that synthesized gold nanoparticles in deionized water for simultaneous electrochemical detection (Figure 2-13). [47] These methods are high precision for fabricating 2D gold nanostructures. However, the physical methods have many disadvantages; (1) they are expensive, (2) they compose

of several complicated steps and set-ups and (3) they could not synthesize 3D nanostructures.
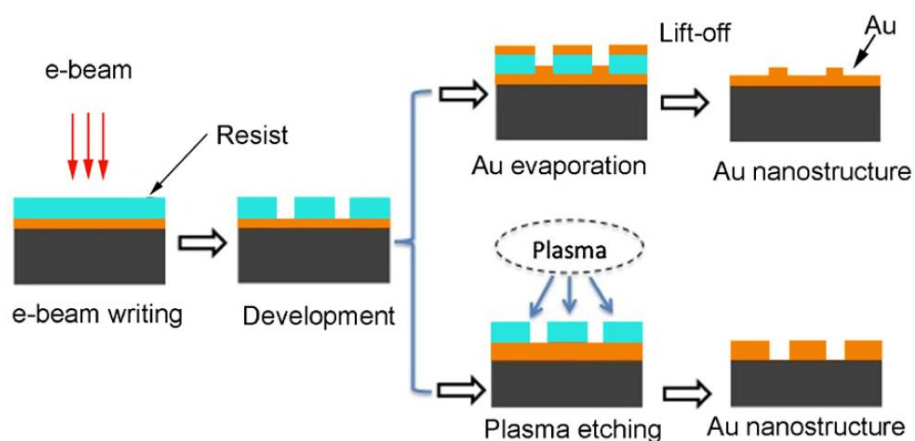
Figure 2-11 Schematic of the processes for the fabrication of nanostructued SERS substrates. Reprinted (adapted) with permission from [45] Copyright (2012) Institute of Physics Publishing.
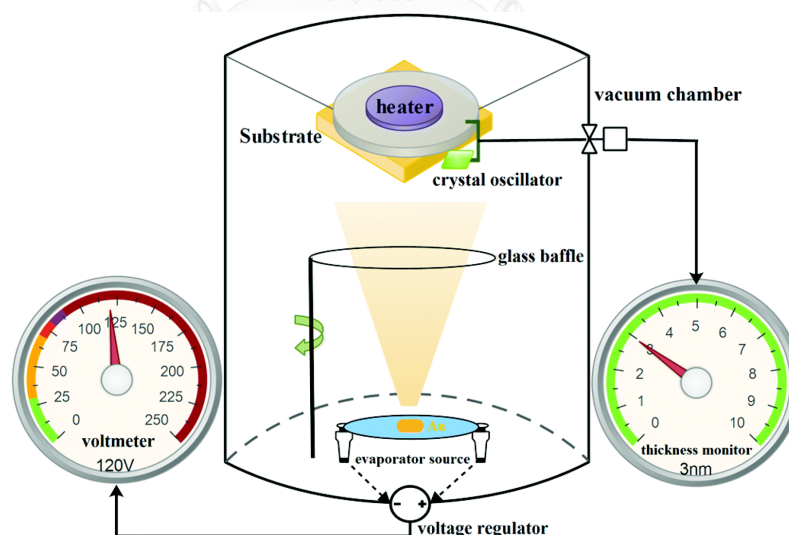
Figure 2-12 The schematic diagram for vacuum thermal evaporation technique to fabricate the ultrathin gold nanoparticles for light trapping in organic photosensitive diodes. Reprinted (adapted) with permission from [46] Copyright (2015) Royal Society of Chemistry.
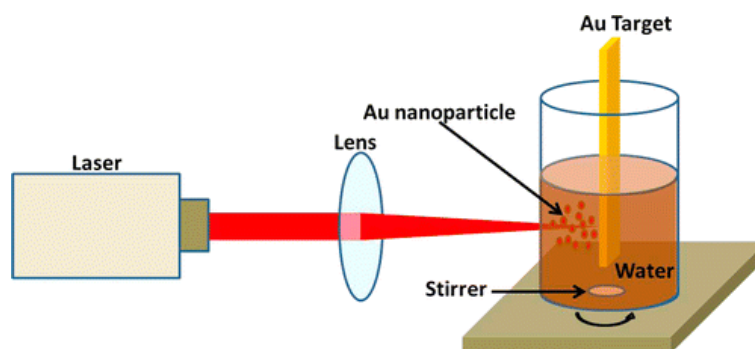
Figure 2-13 Schematic illustration of laser ablating gold target in water for simultaneous electrochemical detection. Reprinted (adapted) with permission from [47] Copyright (2014) American Chemical Society.

2.5.2 Synthesis of AuNPs in chemical approach

Bottom-up process by chemical methods are main method in nanoscience and nanotechnology which produce fancy nanostructures such as one-dimensional (1D) nanowires (NWs), nanorods (NRs), and nanotubes (NTs), two-dimensional (2D) nanoplates, and three-dimensional (3D) hierarchical structures. [48] In the case of AuNPs, the redox reactions between tetrachloroauric ($AuCl_4^-$) and reducing agent play important roles in engineering gold nanostructures. Many reducing agents have been used to produce fancy structures of AuNPs such as hydrogen peroxide (H_2O_2) (Figure 2-14), [49] ascorbic acid ($C_6H_8O_6$) (Figure 2-15), [50] and hydroquinone ($C_6H_6O_2$) (Figure 2-16). [51] $AuCl_4^-$ is easily reduced by weak reducing agents due to the high reduction potential of $AuCl_4^-$, as shown in Eqs. 2-2–2-4. [49-52]

$$AuCl_4^- + 3e^- \rightarrow Au^0 + 4Cl^- \qquad E^o_{re} = +1.002 \text{ V} \qquad \text{(Eq. 2-2)}$$

$$H_2O_2 \rightarrow O_2 + 2H^+ + 2e^- \qquad E^o_{ox} = -0.695 \text{ V} \qquad \text{(Eq. 2-3)}$$

$$C_6H_8O_6 \rightarrow C_6H_6O_6 + 2H^+ + 2e^- \qquad E^o_{ox} = -0.553 \text{ V} \qquad \text{(Eq. 2-4)}$$

$$C_6H_6O_2 \rightarrow C_6H_4O_2 + 2H^+ + 2e^- \qquad E^o_{ox} = -0.700 \text{ V} \qquad \text{(Eq. 2-4)}$$
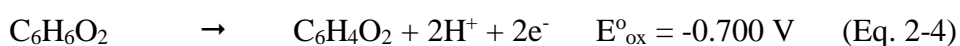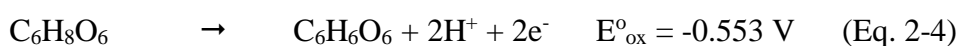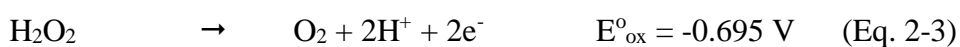
Size and shape of gold as well as other metal nanoparticles as shown in Table 2-1 can be controlled by many synthesis parameters such as reducing agents, metal precursors, solvent, capping agents, and polymeric species for surface protecting agents. These parameters have strong impacted on the crystal growth of metal nanostructures. [53]
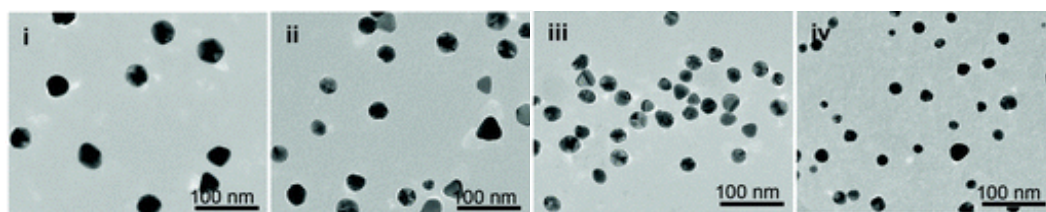
Figure 2-14 TEM images of the nonionic fluorosurfactant-stabilized spherical AuNPs obtained from different concentrations of hydrogen peroxide (i) 0.03, (ii) 0.07, (iii) 0.2, and (iv) 0.6 M. Reprinted (adapted) with permission from [49] Copyright (2012) Royal Society of Chemistry.
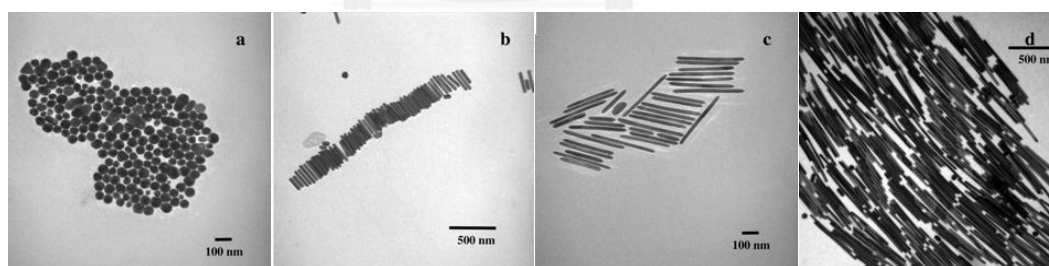
Figure 2-15 TEM micrographs of gold nanorods prepared in the presence of n-alkyl trimethylammonium bromide (CnTAB) such as (a) C10TAB, (b) C12TAB, (c) C14TAB, and (d) C16TAB as capping agent and using ascorbic acid as reducing agent in growth solution. Reprinted (adapted) with permission from [50] Copyright (2003) American Chemical Society.
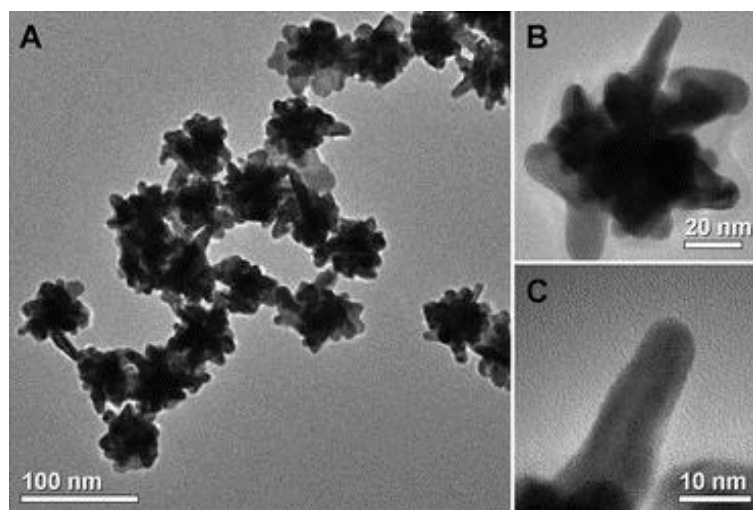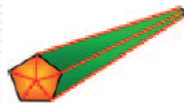
Figure 2-16 TEM micrographs showing formation of gold nanostars using hydroquinone as reducing agent in growth solution. Reprinted (adapted) with permission from [51] Copyright (2011) Royal Society of Chemistry.

Table 2-1 A summary of different morphology of metal nanocrystals. Reprinted (adapted) with permission from [53] Copyright (2009) Royal Society of Chemistry.

Structures	Shapes	Schematic drawing	Metals
Single-crystal	perfect/truncated cube[a]		Pd, Ag, Au, Pt, Cu, Rh, Bi, Fe
	perfect/truncated octahedron[a]		Pd, Ag, Au, Pt
	perfect/truncated tetrahedron[a]		Ag, Au, Pt, Rh
	rectangular bar		Pd, Ag, Pt
	octagonal rod		Pd, Au, Fe, Co, Ni
	rectangular or octagonal wire		Pd, In, Sn, Sb, Fe, Co

Structures	Shapes	Schematic drawing	Metals
Singly twined	right bipyramid		Pd, Ag
	beam		Ag
Multiply twined	detahedron[a]		Pd, Ag, Au
	icosahedron[a]		Pd, Au
	five-fold twined pentagonal rod		Pd, Ag, Au, Cu
	five-fold twined pentagonal wire		Ag, Au, Cu
	Triangular/hexagonal plate		Pd, Ag, Au, Cu, Pb, Bi, Co, Ni
	disc		Sn, Co

[a] Platonic solid

2.6 Growth mechanism of AuNPs

2.6.1 Homogeneous and heterogeneous nucleation

Nucleation is the process which nuclei (seeds) function as templates for crystal growth. Homogeneous nucleation is a situation where nuclei developed uniformly in the parent phase. On the other hand, heterogeneous nucleation is the formation of structure in homogeneities (containing surfaces, impurities, and grain boundaries). [54, 55] The process of homogeneous nucleation is considered thermodynamic process based on Gibbs free energy (ΔG) consisting of bulk free energy (ΔG_V) and surface free energy (σ). [54, 56]

In the homogeneous nucleation, at saturation concentration (C_s) as shown in Figure 2-17a, gold ions were reduced to gold atoms, and started to aggregate into gold clusters (nuclei) due to reducing free energy within the system. The nuclei assemble into nanocrystals or seeds. When the concentration of seeds reacts the highest concentration (C_s), seeds start to accumulate to nanoparticles. [53, 55] The ΔG of homogeneous nucleation (ΔG_{hom}) could calculate as follows: [54, 56]

$$\Delta G_{hom} = \sigma A + \Delta G_V V \qquad \text{(Eq. 2-5)}$$

Where ΔG_V, V, σ and A are bulk free energy per unit volume, volume, surface free energy per unit area, and surface area of the new phase, respectively. V and A depend on the shape of gold nuclei. [56] On the other hand, in the heterogeneous nucleation, if nucleation occurred in a system containing pre-synthesized nanocrystals or seeds, the ΔG can be significantly changed. [55] The ΔG of heterogeneous nucleation (ΔG_{het}) could calculate as follows: [54, 56]

$$\Delta G_{het} = \Delta G_{hom}\left(\frac{f}{2}\right) \qquad \text{(Eq. 2-6)}$$

Normally, ΔG$_{het}$ was less than ΔG$_{hom}$ due to the term of energy reduction factor (f). If the new nuclei can wet with adding nanocrystal or seed, supersaturation concentration of nanocrystal or seed is not required for nucleation, as shown in Figure 2-17b. Nanopartilces in this system consume nanocrystal or seed at a concentration less than the supersaturated concentration for homogeneous nucleation. [55, 56]
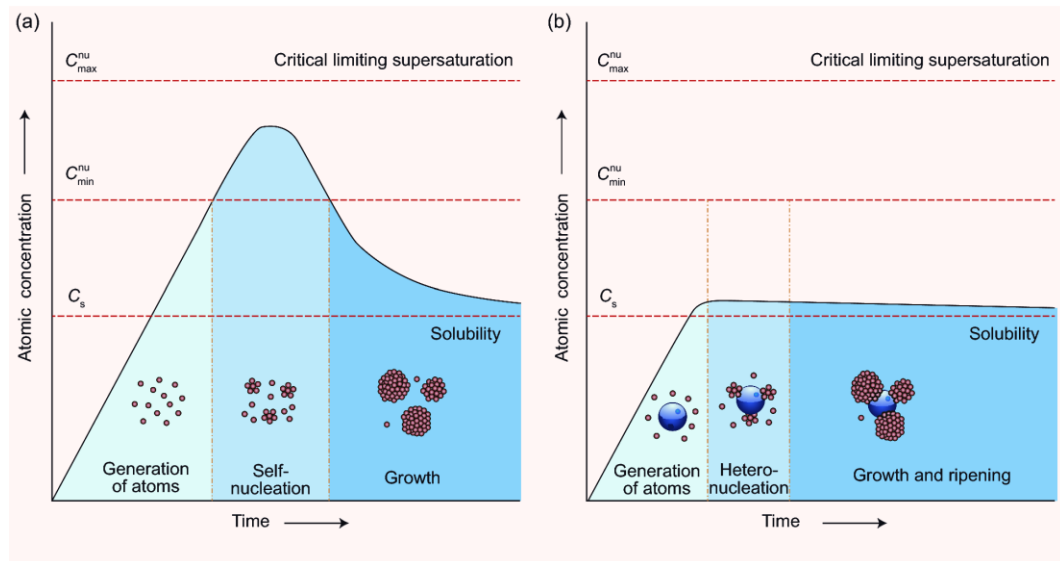
Figure 2-17   Schematic illustrations involved in the formation of nanoparticles through (a) homogeneous nucleation and (b) heterogeneous nucleation. Reprinted (adapted) with permission from [55] Copyright (2015) Oxford University Press.

2.6.2   LaMer Mechanism

This mechanism explain the formation of crystals by seperation the process into seed generation, nucleation and growth. The process of nucleation and growth were explined by the LaMer mechanisum, as shown in Figure 2-17a. (1) a rapid generation of gold atom produced large number of nuclei in solution. (2) number of nuclei were raplidly increase with a concomitant drop in the concentration of gold ions. (3) after the nucleation, the growth of particles were controlled by the diffusion process. [54]

2.6.3 Orientated attachment

The orientated attachment occures as two primary nanoparticles jointed together by the same crystalline facet, as shown in Figure 2-18. [57] The attached particles will adjustment and accumulation with each other until the crystallographic orientation of the two crystals matched. The two particles must be within 0.5-1.0 nm vicinity of each other for orientated attachment to occur. The Coulombic force was proposed as the major driving force for this attraction. [54, 58]
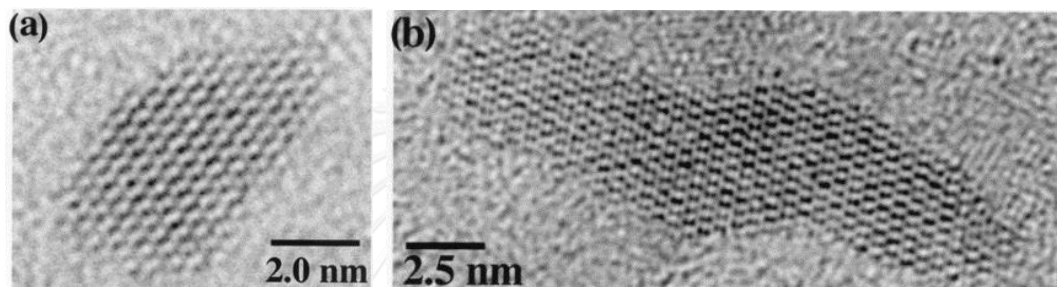
Figure 2-18 Progression of chain development in titania crystallites: (a) single primary crystallite and (b) four primary crystallites forming a single crystal via oriented attachment. Reprinted (adapted) with permission from [58] Copyright (1999) Elsevier.

2.6.4 Crystal growth pattern

By LaMer growth mechanism, during the nucleation step, the maximum concentration of metal atom in system or supersaturation will control the crystal growth of metal nanoparticles. [53] That means the patterns of metal atom deposition on metal nanoparticles such as dislocation-driven, layer-by-layer and dendritic growth was controlled by the supersaturation as shown in Figure 2-19. [59]
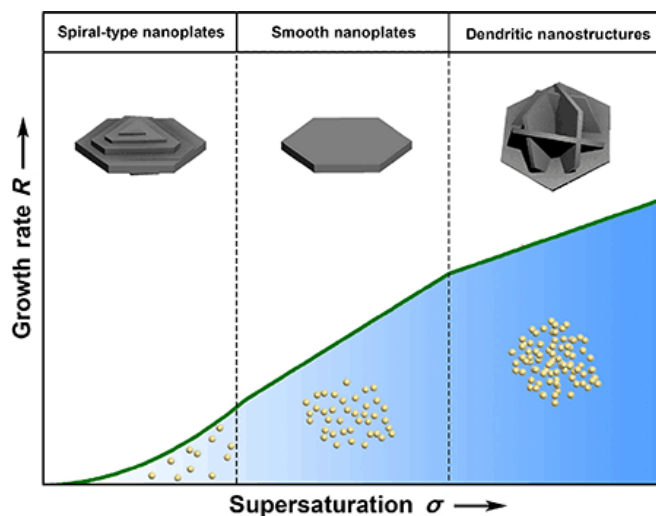
Figure 2-19 Schematic illustrations for growth rate of different crystal growth pattern comparison with supersaturation concentrations. Reprinted (adapted) with permission from [59] Copyright (2015) Springer.

2.7 Dendritic growth

At high supersaturation (Figures 2-17a and 2-19), the dendritic growth mechanism is prominent for controlling the growth of crystal in the system. The high precursor flux at the crystal surface promoted non-equilibrium monomer aggregation. The rate of diffusion from the surrounding environment limits the crystal growth on surface or diffusion-limited aggregation (DLA). Moreover, kinks or corners of the crystal have the highest concentration flux between the high-supersaturation reaction media and the crystal surface. Therefore, the growth rate in these positions is the fastest, which usually generates crystals with rough surfaces and fractal patterns like snowflakes. [48] In dendritic gold nanostructures,these structures have the characteristics of trunk and brunches with single crystals with a (111) plane and grew angle $\sim 60^{\circ}$ which refers to the crystal growth along the $\langle 211 \rangle$ direction as shown in Figure 2-20. [60]

The dendritic gold nanostructures were widely used as substrate in surface-enhanced Raman scattering (SERS) for trace chemical analysis because a large of electric field enhancement or "hot sport" was formed on tips and corners of dendritic structures. Many chemical compounds from low concentration to single molecules such as rhodamine 6G (R6G), [13] rhodamine B (RhB) [61] and *p*-aminothiophenol (PATP) [62] could be detected SERS signals by dendritic gold nanostructures. Moreover, dendritic gold nanostructures could change and develop to other structures such as flower-like, urchin-like and meat ball-like structure as shown in Figure 2-21. [62]
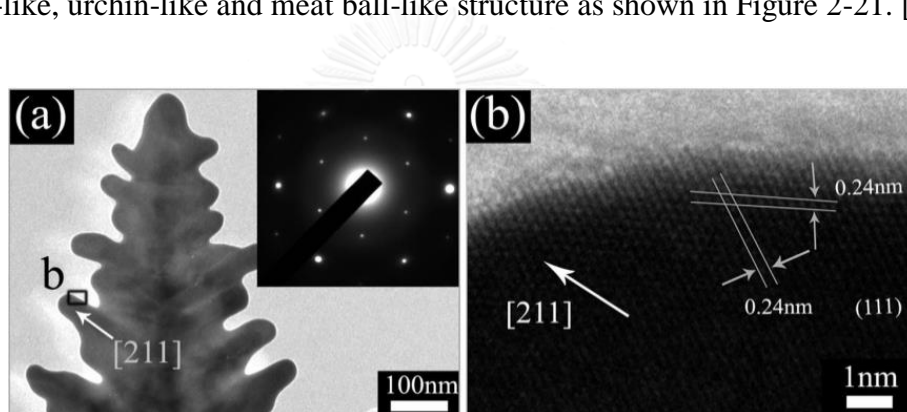
Figure 2-20   (a) A typical TEM image of trunk with symmetric leaves of dendritic gold nanostructure (the inset shows the corresponding SAED pattern). (b) HRTEM of the area marked in (a). Reprinted (adapted) with permission from [60] Copyright (2011) American Chemical Society.
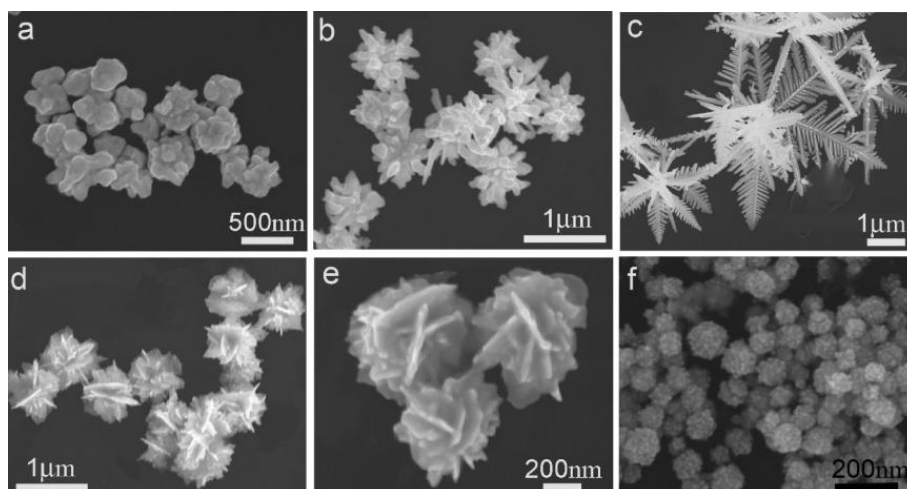
Figure 2-21 SEM images of structural evolution of dendritic growth from (a) irregular shape to (b) urchin-like, (c-e) flower-like, and (f) meat ball-like gold nanostructures under variation concentration of shape controlling agents. Reprinted (adapted) with permission from [62] Copyright (2009) American Chemical Society.

CHAPTER III
EXPERIMENT

3.1   Chemicals and materials

1. Ammonium hydroxide (NH_4OH), 25% (w/w), Merck (Thailand)

2. Hydrochloric acid (HCl), 37% (w/v), Merck (Thailand)

3. Sodium chloride (NaCl), Merck (Thailand)

4. Hydrogen peroxide (H_2O_2), 30% (w/w), Merck (Thailand)

5. Nitric acid (HNO_3), 25% (w/w), Merck (Thailand)

6. Sodium nitrate ($NaNO_3$), Merck (Thailand)

7. Silver nitrate ($AgNO_3$, purity $\geq$ 99.8%), Merck (Thailand)

8. Tetrachloroauric (III) acid ($HAuCl_4$), Sigma-Aldrich

9. Sodium borohydride ($NaBH_4$), Merck (Thailand)

10. Rhodamine 6G (R6G), Sigma-Aldrich

11. Spherical gold nanoparticles (size~20 nm, O.D. =1), Sigma-Aldrich

All chemicals were analytical grade and were used as received. Deionized (DI) water was used as a solvent throughout this study. All glassware was cleaned with detergent and soaked in *aqua regia* for 30 min before thoroughly rinsing with DI water several times before using. A great caution was always implemented when dealing with the highly corrosive aqua regia: a mixture of concentrated HCl and HNO_3 at a volume ratio of 3:1.

3.2   Instruments

1. Ocean optics USB4000 fiber optic spectrometer

2. Hitachi Model H-7650 transmission electron microscope

3. JEOL JSM-6510 scanning electron microscope coupled with energy dispersive X-Ray (EDX) detector

4. Thermo scientific DXR Raman microscope

3.3   Synthesis of UL-AuMSs

UL-AuMSs were synthesized by a one-pot procedure with H_2O_2 as a reducing agent without a stabilizer as shown in Figure 3-1. Briefly, H_2O_2 solution (9 M, 3 mL) with added $AgNO_3$ (5–400 μM) was rapidly syringe-injected into a test tube containing $HAuCl_4$ solution (0.5 M, 3 μL). The mixture was vortexed for 20 s before leaving undisturbed. The yellow $HAuCl_4$ solution turned blue-green before precipitating as reddish-brown gold particles. During a 5-min reaction period, a liberation of small bubbles indicated a progress of the redox reaction. The precipitated gold particles were collected by decantation of supernatant. The particles were soaked in NH_4OH solution (5 M, 3 mL) under ultrasonic in order to remove AgCl film by changing into a water-soluble silver-amine complex. The gold particles were centrifugally separated before thoroughly washed with DI water several times.
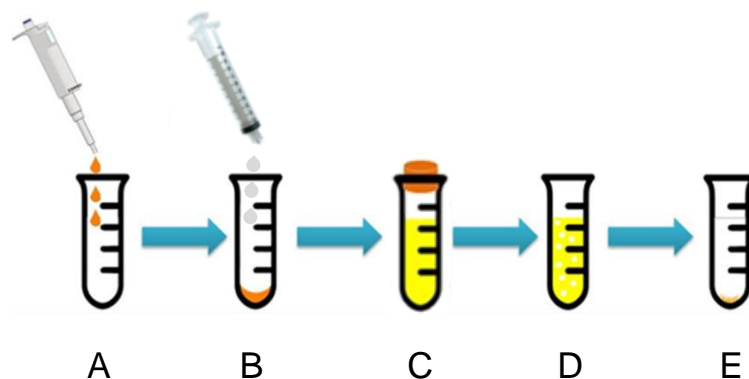
Figure 3-1 Schematic illustration shows sequence of operations for the synthesis of UL-AuMSs: (A) loading of $HAuCl_4$, (B) injection of Ag^+ containing H_2O_2, (C) vortex (D) precipitation and separation, (E) cleaning with NH_4OH.

3.4   SEM Characterization

All SEM images were taken under at high vacuum mode using acceleration voltages of 10–30 kV with secondary electron imaging (SEI) detector. Elemental analysis was carried out using an energy dispersive X-ray spectrometer (EDS). The gold microstructures were deposited onto a carbon tape attached on a stainless steel stub for SEM analysis. For time-dependent SEM investigation, the UL-AuMSs were rapidly transferred onto a carbon tape by a flash-flow technique. Briefly, at a pre-determined time, an aliquot of 10 μL of the reacting solution was dispensed onto a tilted carbon tape-covered stub. The UL-AuMSs stuck on the carbon tape was immediately dried by an air jet. The adhered UL-AuMSs were cleaned by a continuous flow of DI water. The specimen was vacuum dried before SEM imaging. The adhered particles on carbon tape were cleaned by a continuous flow of DI water and vacuum dried before further characterization.
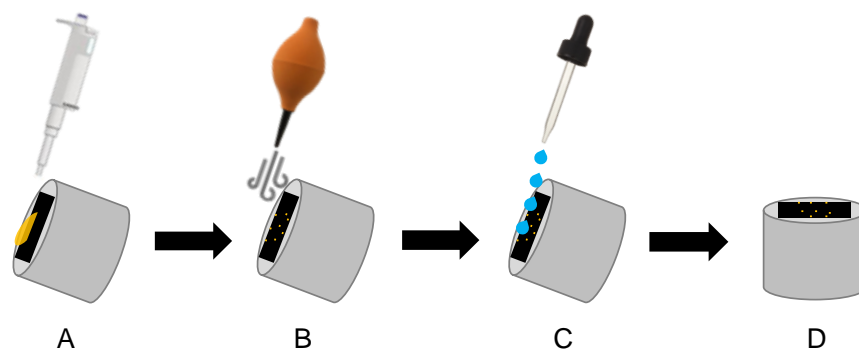
Figure 3-2   A Schematic illustration of a flash-flow sampling of UL-AuMSs for time dependent SEM investigation: (A) deposition of UL-AuMSs on tilted stub, (B) air jet drying, (C) washing, and (D) vacuum dried.

3.5   SERS measurement

All SERS spectra were collected by Raman spectrometer using 50x objective with a spot size of ~1 µm. Diode laser with 532 nm excitation wavelength at 0.1 mW was employed. The measurements were conducted with 1 s exposure time and 128exposure numbers. To prepare a specimen for SERS measurement, the NH_4OH-cleaned UL-AuMSs (~0.3 mg) were incubated in R6G solution (0.01 nM–1 µM, 3 mL) for 15 min before centrifugal separation. The R6G-immobilized UL-AuMSs were cleaned with DI water twice in order to remove the un-bound R6G.The cleaned R6G-immobilized UL-AuMSs were suspended in deionized water before deposition on an aluminum foil or gold microplate-coated carbon tape for SERS measurement.

3.6   Monitoring the shape evolution of HS-AuMSs

Hemi-spherical gold microstructures (HS-AuMSs) were synthesized by the reduction of $HAuCl_4$ using H_2O_2 as a reducing agent without any stabilizer. A clear polyethylene box (5×5×0.5 cm) with mica sheet was set as shown in Figure 3-2. Then,

the test tube containing HAuCl$_4$ solution (0.5 M, 30 μL) was rapidly syringe-injected into H$_2$O$_2$ solution (9 M, 3 mL). The mixture was vortexed for 20 s and suddenly transferred to setting box (Figure 3-3) before leaving undisturbed. The yellow HAuCl$_4$ solution turned blue-green before precipitating as reddish-brown gold particles. The gold particles deposited on mica sheet were rinsed by DI water several times before transferred onto carbon tape on a stainless steel stub for SEM analysis. The sampling spots on mica sheet (A-B, Figure 3-3) were 1-cm apart.
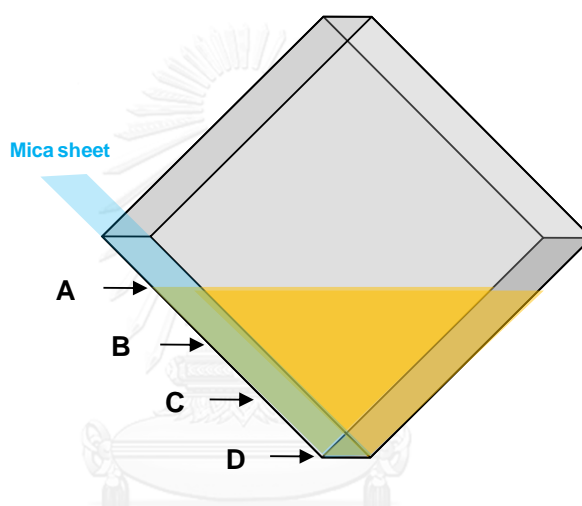
Figure 3-3   Schematic illustration for monitoring the shape evolution of HS-AuMSs.

3.7   Synthesis of UL-AuNPs

Urchin-like gold nanoparticles (UL-AuNPs) were synthesized without a stabilizer via a one-pot procedure using H$_2$O$_2$ as a reducing agent. H$_2$O$_2$ (9 M, 3 mL) with 25 μM of AgNO$_3$ was poured into a test tube containing HAuCl$_4$ (0.5 M, 0.3 μL) and spherical gold nanoseeds (150 μL). The yellow HAuCl$_4$ solutions transformed into a blue-green solution as UL-AuNPs were generated. The colloid was diluted to 0.1 mM by DI water for UV-Vis measurement. A solution of 1 μL UL-AuNPs was deposited and dried on a carbon coated grid for TEM analysis.

CHAPTER IV
RESULTS AND DISCUSSION

4.1 Reducing capability of H_2O_2

H_2O_2 is well-known as oxidizing agent. However, under appropriate conditions, it can act as mild reducing agent. There are many reports demonstrated that H_2O_2 was employed as an efficient reducing agent for fabrication of gold nanosheets [52] and gold nanoparticles (AuNPs). [63] In this work, H_2O_2 was employed as the sole reducing agent for the design and manipulation of UL-AuMSs with trace Ag^+ as the shape controlling agent (Figure 4-1). H_2O_2 can turn Au^{3+} as the pale yellow mixture of H_2O_2 and Au^{3+} into colorless of UL-AuMSs within 5 min. The reduction of $HAuCl_4$ by H_2O_2 in acidic condition was reported elsewhere as Eqs. 3-1–3-3. [52, 63, 64]

$$AuCl_4^- + 3e^- \quad \rightarrow \quad Au + 4Cl^- \qquad E^o_{re} \; = + 1.002 \text{ V (Eq. 3-1)}$$

$$H_2O_2 \quad \rightarrow \quad O_2 + 2H^+ + 2e^- \qquad E^o_{ox} \; = - 0.695 \text{ V (Eq. 3-2)}$$

$$2AuCl_4^- + 3H_2O_2 \quad \rightarrow \quad 2Au + 3O_2 + 8Cl^- + 6H^+ \quad E^o_{cell} = + 0.307 \text{ V (Eq. 3-3)}$$
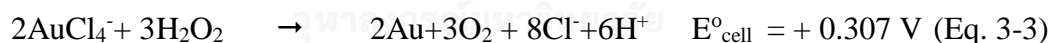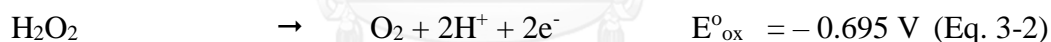
The reddish-brown precipitate, which is a signature of gold micro particles [65], was quasi-sphere gold microstructures (QS-AuMSs) with average particle size of 1.8 µm (Figure 4-1A). The high concentration of H_2O_2 facilitated a rapid reduction of Au^{3+} while the absent of stabilizer promoted the formation of the highly stable quasi-sphere gold microstructures. [63] However, H_2O_2 cannot reduce Ag^+ into silver atom under an acidic condition. [66, 67] There was neither reaction nor product when silver nitrate was mixed with H_2O_2 (Figure 4-1B). When Au^{3+} solution was mixed with Ag^+ solution, solid AgCl instantaneously precipitated as chain-like aggregates of ~0.2 µm primary

particles (Figure 4-1C). The chain-like structures were AgCl as it withstood HNO_3 but instantaneously dissolved in NH_4OH (data not shown). [68, 69] When a solution of H_2O_2 with trace Ag^+ was mixed with a solution of Au^{3+}, the pale yellow mixture of H_2O_2 and Au^{3+} turned colorless within 5 min with a concomitant precipitation of reddish-brown gold particles. The precipitants were ~1.8 μm UL-AuMSs with a uniform distribution of ~700 nm thorn on their surfaces (Figure 4-1D). Interestingly, the chain-like structures of AgCl were not observed in Figure 4-1D. Instead, AgCl film was detected on gold surface as confirmed by SEM-EDS measurements (Figure 4-2). The results in Figure 4-1 and Figure 4-2 suggested that Ag^+ involved in the formation and growth of the thorn structures.
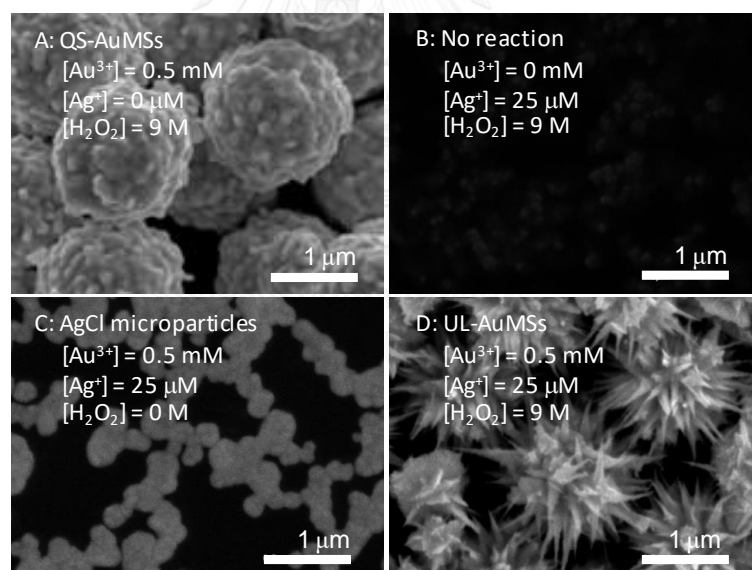
Figure 4-1   SEM images of products from the reaction of Au^{3+}, Ag^+, and H_2O_2: (A) QS-AuMSs, (B) No reaction, (C) chain-like AgCl microparticles, and (D) UL-AuMSs. The reaction ingredients are shown in the figures. Scale bars indicate 1 μm.
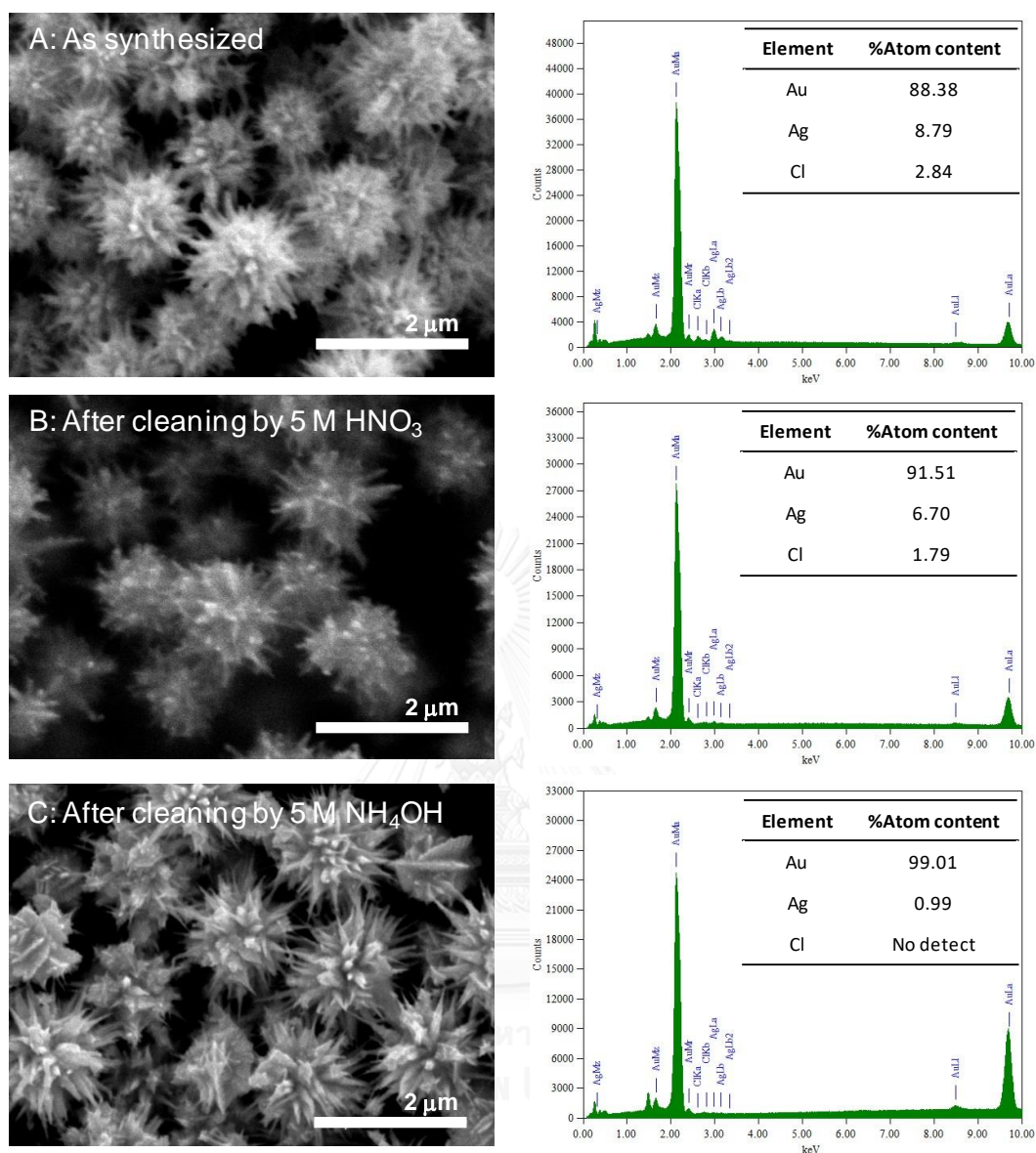
Figure 4-2 SEM images, EDS spectra, and elemental composition of UL-AuMSs: (A) as-synthesized, (B) after cleaning with 5 M HNO_3 and (C) after cleaning with 5 M NH_4OH. The UL-AuMSs were synthesized using 0.5 mM Au^{3+}, 9 M H_2O_2, and 25 μM Ag^+. As confirmed by EDS spectra and elemental compositions, AgCl physically adsorbed on the surface of as-synthesized UL-AuMSs. AgCl do not dissolve in HNO_3 of any concentration but effortlessly dissolves in NH_4OH.

4.2   The influences of Ag$^+$ on UL-AuMSs

To gain an insight understanding on the roles of trace Ag$^+$, firstly, we explore the optimal concentration of Au^{3+} and H$_2$O$_2$ for UL-AuMSs fabrication. Under a fixed concentration of Ag$^+$ at 25 μM and low concentration of Au^{3+} at 0.5 mM, the UL-AuMSs were obtained (Figure 4-3A–3C). The particle size and thorn length increased with increasing H$_2$O$_2$ concentration. Note: the maximum concentration of commercially available analytical grade H$_2$O$_2$ is 30% w/w (~9.8 M). At higher concentrations of Au^{3+} (2.5 and 5.0 mM) the flower-like gold microstructures (FL-AuMSs) were obtained (Figure 4-3D–3I). The complexity of the flower-like structures increased with increasing H$_2$O$_2$ concentration.
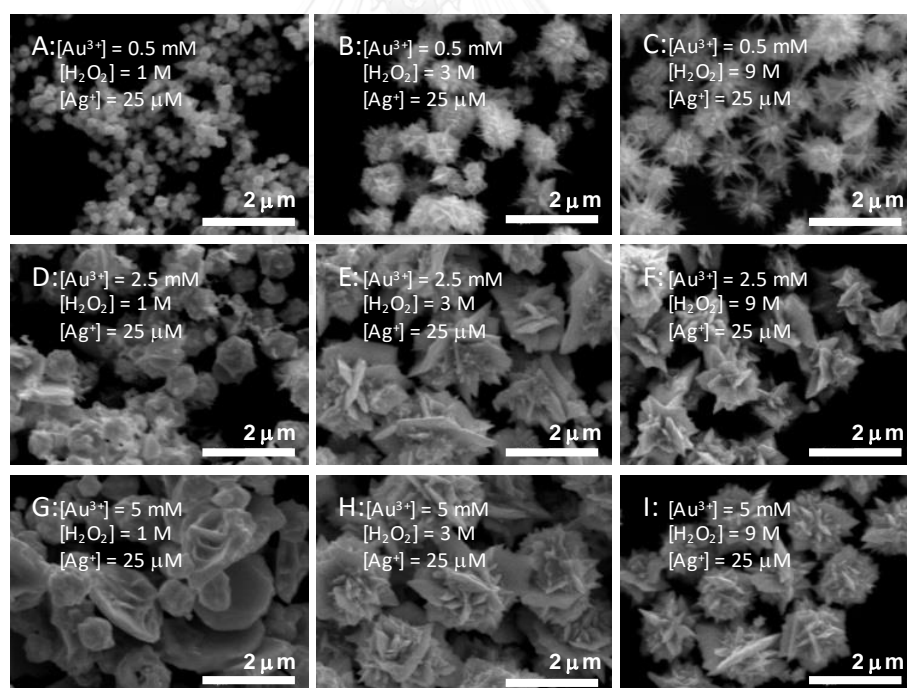
Figure 4-3   SEM images show variation of gold microstructures at various concentrations of Au^{3+} and H$_2$O$_2$ under a fixed concentration of Ag$^+$ (25 μM). The reaction ingredients are shown in the figures. Scale bars indicate 2 μm.

At high concentration of H_2O_2 (9 M), the reactions completed within 5 min confirmed by clear solution of supernatant after adding $NaBH_4$, while those at lower concentrations (0.5 and 1 M) completed within 30 min. The QS-AuMSs were always obtained in the systems without Ag^+ as shown in Figure 4-4. The quasi-spherical shape synthesized at 3 and 9 M of H_2O_2 with narrow size distribution suggests a complete separation of the nucleation and growth periods. [70, 71]
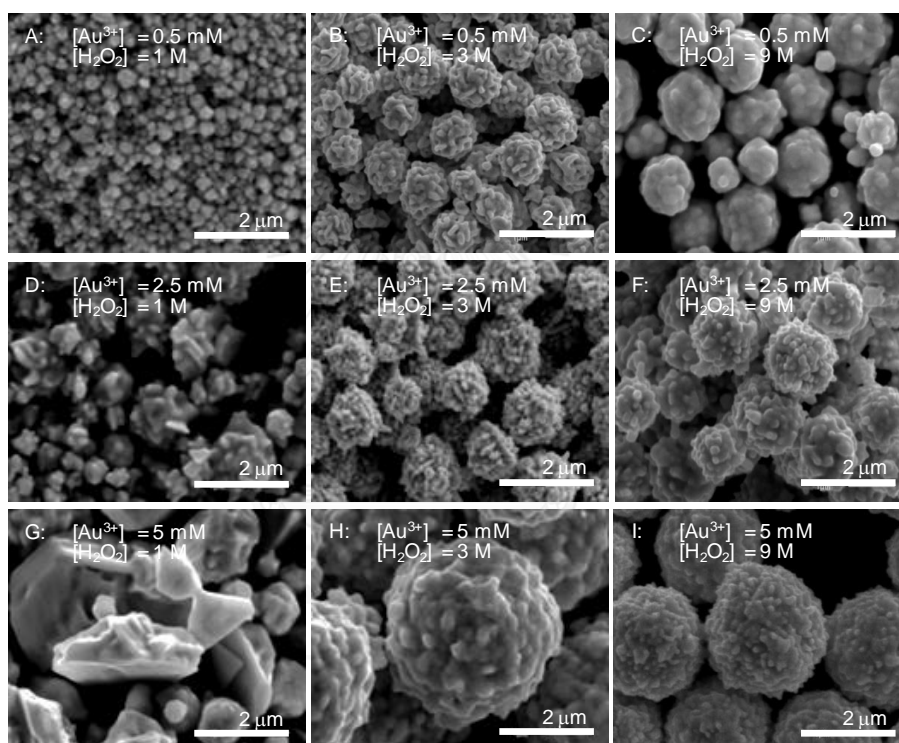
Figure 4-4   SEM images show variation of gold microstructures at various concentrations of Au^{3+} and H_2O_2. The reaction ingredients are shown in the figures. Scale bars indicate 2 μm.

Based on the microstructure shown in Figure 4-3C, a high concentration of H_2O_2 (9 M) and low concentration of Au^{3+} (0.5 mM) were necessary for the fabrication of UL-AuMSs. Gold microstructures as FL-AuMSs synthesized at low concentration of H_2O_2 (1 and 3 M) were obtained in Figure 4-5A and 4-5B, respectively. When a

moderate concentration of H_2O_2 (7 M) was employed, gold microstructures with petals and thorns were produced (Figure 4-5C). As a result, we used 9 M H_2O_2 and 0.5 mM Au^{3+} with different concentrations of Ag^+ for our further investigation.
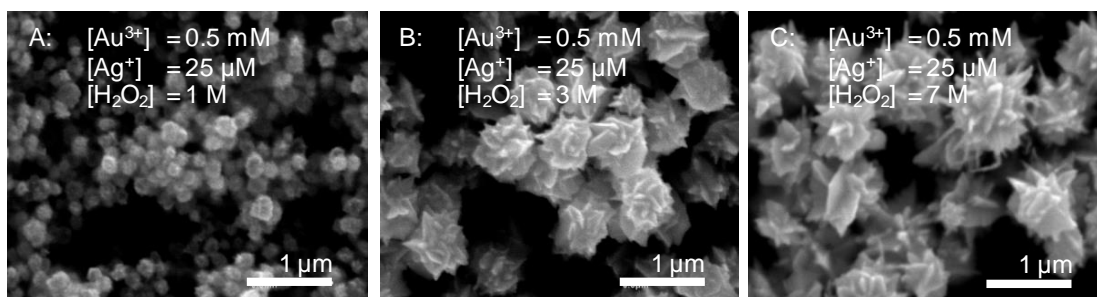
Figure 4-5   SEM images of gold microstructures synthesized using (A) 1 M, (B) 3 M and (C) 7 M H_2O_2. The concentration of Au^{3+} and Ag^+ were kept constant at 0.5 mM and 25 μM, respectively. These microstructures contained both petals and nanothorns.

Figure 4-6 shows structural evolution of UL-AuMSs as the concentration of Ag^+ was increased up to 300 μM. The thorn structures developed when Ag^+ was presented. Without Ag^+, QS-AuMSs with an average particle size of 1.8 μm were generated (Figure 4-6A). When Ag^+ concentrations were increased, UL-AuMSs of smaller particle sizes and shorter thorn lengths were obtained. The UL-AuMSs with a maximum particle size of ~1.8 μm and thorn length of ~700 nm were produced using 25 μM Ag^+ (Figure 4-6B). At this concentration, solid AgCl was not observed with the precipitated UL-AuMSs. Interestingly, the particle sizes and thorn lengths decreased with an increase of Ag^+ concentration. At 300 μM Ag^+ (Figure 4-6I), small UL-AuMSs with particle size of ~130 nm and thorn length of ~30 nm developed together with a formation of solid AgCl. At 400 μM Ag^+, a milky white AgCl colloid was obtained without any UL-AuMSs.
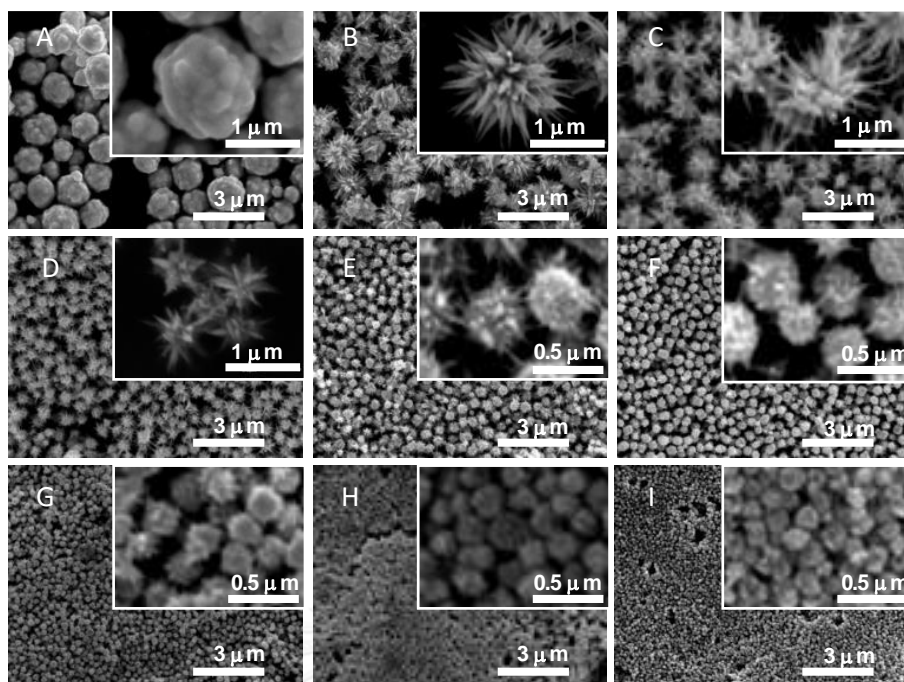
Figure 4-6   SEM images show structural change of UL-AuMSs as the concentration
of Ag$^+$ was increased: (A) 0, (B) 25, (C) 50, (D) 75, (E) 100, (F) 150,
(G) 200, (H) 250 and (I) 300 μM. The concentration of Au^{3+} and H$_2$O$_2$
were kept constant at 0.5 mM and 9 M, respectively. The insets show
enlarged images. Scale bars indicate 3 μm.

After a dissolution of solid AgCl by NH$_4$OH, the colloid turned bluish indicating
the existence of large gold nanospheres. At relatively low concentrations of Ag$^+$ (5 and
10 μM), QS-AuMSs with small buds (short thorns) were developed (Figure 4-7). The
observed phenomena suggested that trace Ag$^+$ induced the formation of thorn
structures. However, a high concentration of Ag$^+$ (at least 25 μM) was necessary for
the formation of long nanothorns. From the results as shown in Figure 4-6 and Figure
4-7, Ag$^+$ did not only initiate the formation of thorn structures but also restrict the
elongation of thorn at high concentration (*i.e.,* greater than 25 μM). Table 4-1

summarizes the particle sizes, thorn lengths and number of thorns per particle of the synthesized UL-AuMSs.
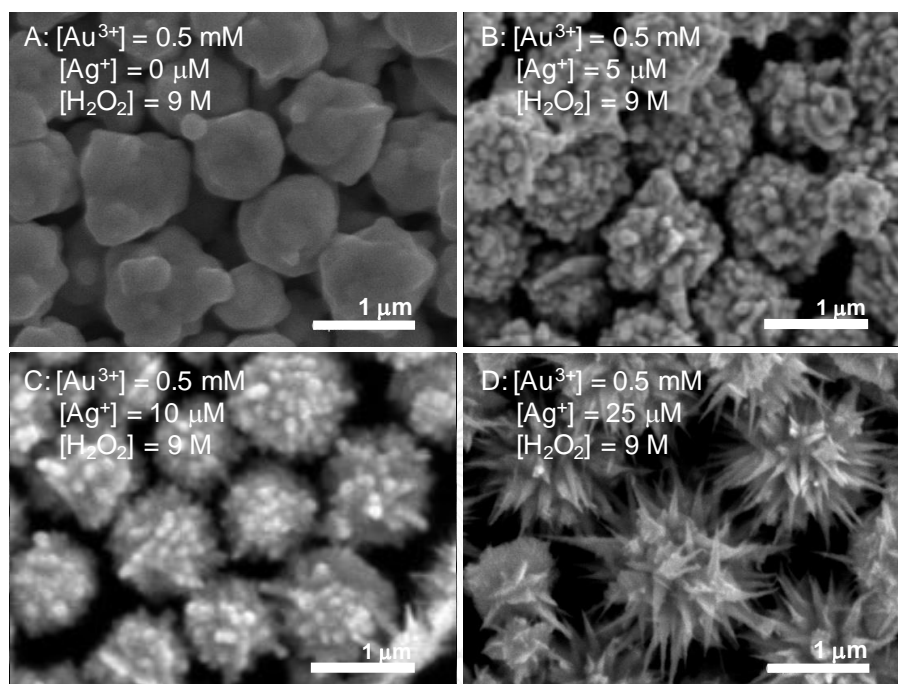
Figure 4-7   SEM images of gold microstructure synthesized using (A) 0, (B) 5, (C) 10, and (D) 25 μM Ag$^+$ as the shape controlling agent. The concentrations of Au^{3+} and H$_2$O$_2$ were kept constant at 0.5 mM and 9 M, respectively.

Table 4-1   Average diameters and average thorn lengths of UL-AuMSs shown in

Figure 4-6. (The data were calculated from 150 particles).

Fig.	$[Ag^+]$ (μM)	Particle diameter (d, nm)	Thorn length (l, nm)	Number of thorns per particle
A	0	1855±330	-	-
B	25	1799±317	708±127	64±13
C	50	1330±314	638±130	52±8
D	75	550±81	288±47	40±5
E	100	410±55	187±43	26±5
F	150	389±60	166±40	14±5
G	200	240±34	99±26	11±2
H	250	193±35	60±10	10±2
I	300	129±26	32±6	4±2

4.3   The growth mechanism of UL-AuMSs

To follow the development of QS-AuMSs and UL-AuMSs, we performed time-dependent SEM investigations using a flash-flow deposition technique to attach the growing microstructures onto carbon tapes. The sample synthesized under the same condition of Figure 4-6B (0.5 mM Au^{3+}, 9 M H_2O_2, and 25 μM Ag^+) was investigated since it provided UL-AuMSs with the longest thorn length. In the system without Ag^+, the small FL-AuMSs (Figure 4-8A1) grew into more complexes and bigger flower-like structures (Figure 4-8A2 and 8A3).
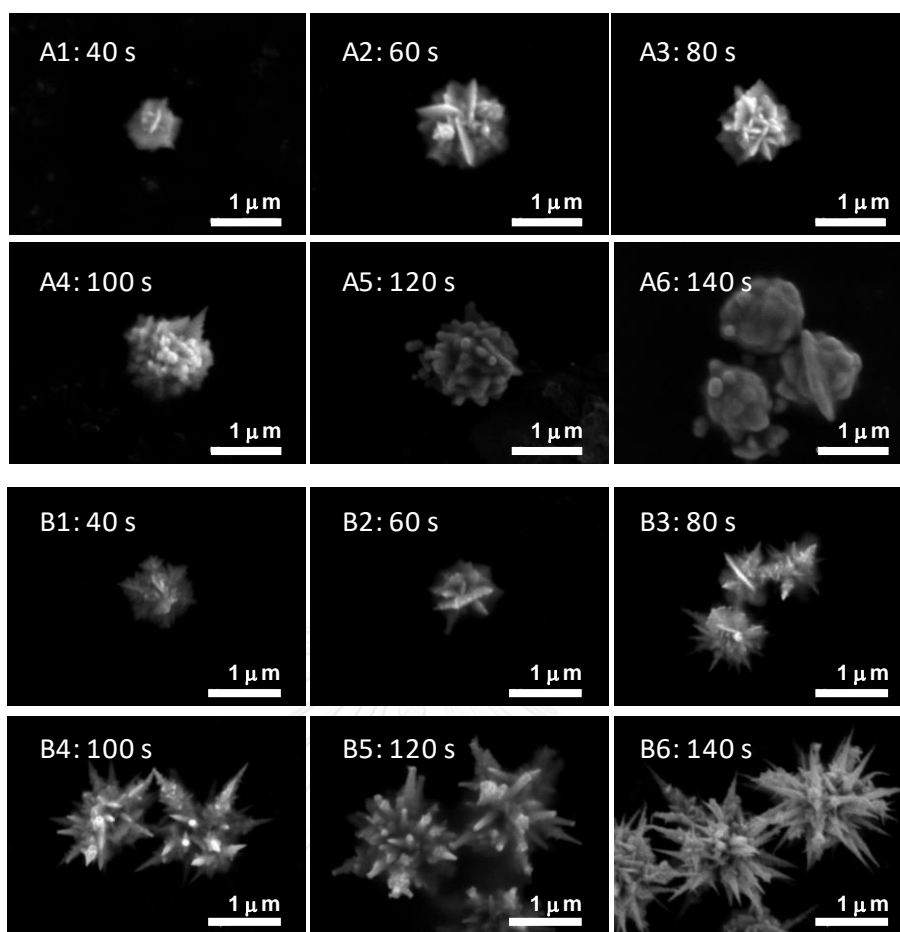
Figure 4-8 SEM images show time-dependent structural evolution of gold microstructures: (A) QS-AuMSs without Ag$^+$ and (B) UL-AuMSs with 25 μM Ag$^+$. The concentration of Au^{3+} and H$_2$O$_2$ were kept constant at 0.5 mM and 9 M, respectively. The scale bars indicate 1 μm.

The small FL-AuMSs perpendicularly grew on a basal plane. The development of perpendicular petal structures was due to the stress relief mechanism *via* an introduction of structure with large lattice mismatch. [72, 73] The further growth induced an aggregated attachment and deposition of AuNPs to fill the gaps between petals (Figures 4-8A4 and 4-8A5). Finally, the QS-AuMSs were obtained while the gaps were fully filled (Figure 4-8A6). Surprisingly, in the system with trace Ag$^+$, we

found that UL-AuMSs were also developed from small FL-AuMSs (Figures 4-8B1 and 4-8B2). The TEM images and SAED suggested that the petals of small FL-AuMSs were gold nanosheets with (111) basal planes (Figure 4-9). The crystal facets are directly related with interplanar spacing (d) which calculated from distance between two bright spots of SAED pattern (R) as follows:

$$d = \frac{2}{R} \quad \text{(Eq. 3-4)}$$

The d values were calculated form SAED pattern (Figures 4-9A–C (inserted figures)) as ~2.4 Å that is characteristic of (111) lattice spacing of the fcc Au crystal. [13, 60]
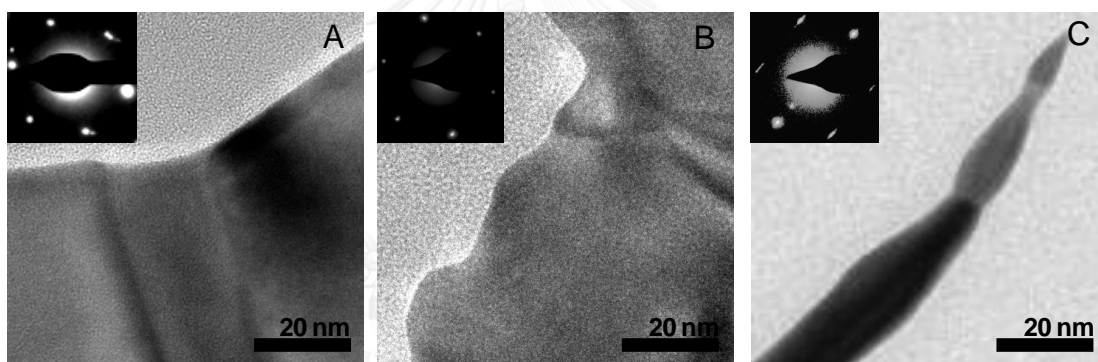
Figure 4-9   TEM images with insert SAED images of gold nanopetals after a 40-s reaction time from the systems: (A) without Ag^+ and (B) with 25 μM Ag^+. (C) A gold nanothorn after a 140-s reaction time from the system with 25 μM Ag^+. The concentration of Au^{3+} and H_2O_2 were 0.5 mM and 9 M, respectively.

The small petals developed into thorn structure due to the deposition of AuNPs at the tip of the trunks instead of filling in the gaps or bound onto the (111) facets. The deposited AuNPs underwent via aggregated attachment, grains rotation, and grains relaxation (Figure 4-10) [74] as the thorn grew under an assistance of Ag^+.

Aggregates attachment

⇩

Grains rotation

⇩

Grains relaxation
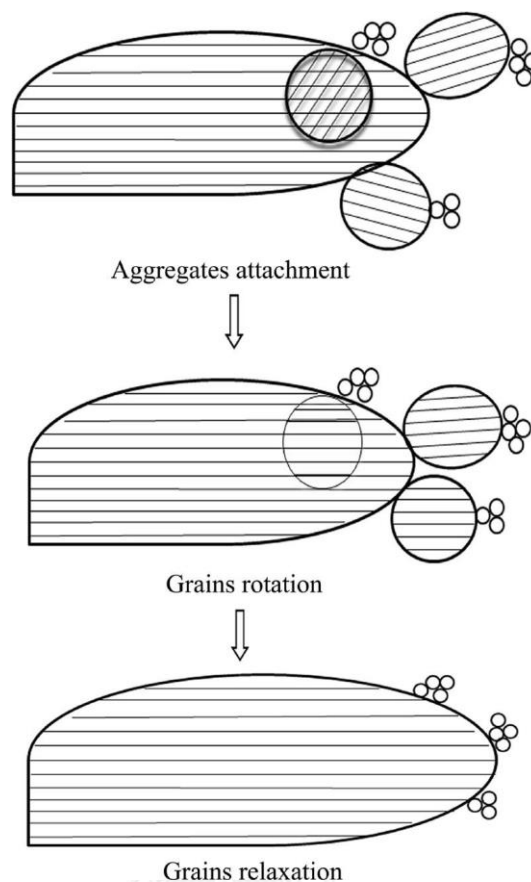
Figure 4-10   Schematic representation shows the proposed morphological and structural evolution during a dendrite growth. Reprinted (adapted) with permission from [74]. Copyright (2012) American Chemical Society.

Within 140 s, FL-AuMSs transformed into fully developed UL-AuMSs (Figures 4-8B3–B6). SEM-EDS images suggested that the UL-AuMSs were covered by solid AgCl (Figure 4-11). It was proven that Cl$^-$ is preferentially adsorbed on Au (111) facets especially for those of nanoplates and nanosheets. [75, 76] The added Ag$^+$ reacted with Cl$^-$ and formed solid AgCl which physically adsorbed on the surface of the petals/thorns. [17, 18] The adsorbed AgCl altered the growth pathway of petals as it prevented the deposition of AuNPs on Au (111) facets. The TEM images and SAED

confirmed that the nanopetals and nanothorns were covered with (111) facets (Figure 4-9).
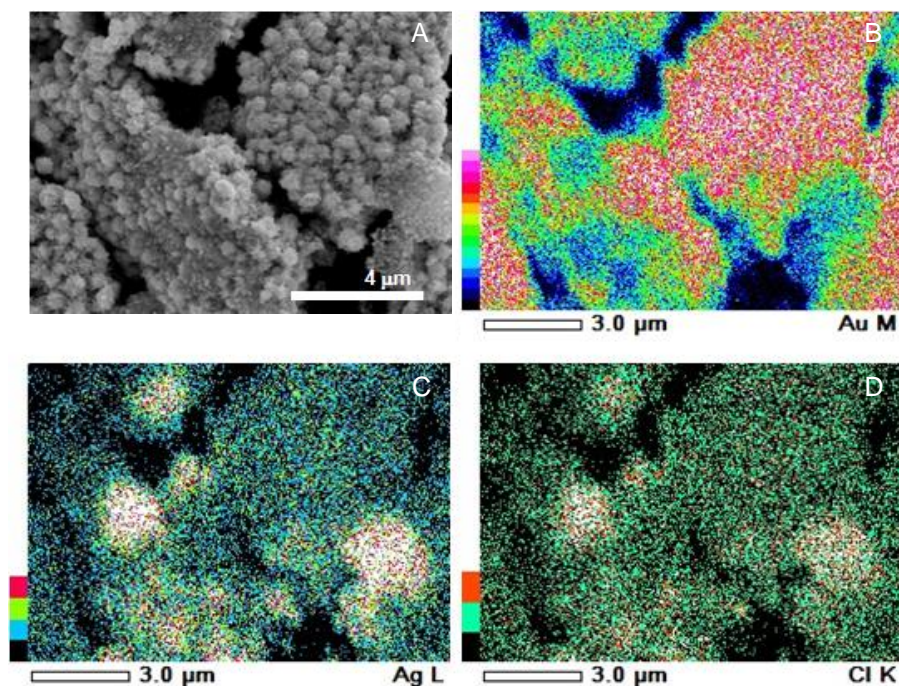
Figure 4-11 (A) An SEM image of UL-AuMSs and the corresponding EDS elemental maps of (B) Au, (C) Ag, and (D) Cl. A good correlation between Ag-map and Cl-map confirm the formation of AgCl on the gold surface. The UL-AuMSs were synthesized using 0.5 mM Au^{3+}, 9 M H_2O_2, and 100 µM Ag^+.

AgCl seemed to play a major role on the development and growth of the nanothorn structures. Without Ag^+, Figure 4-12A, the nanopetals showed a unique dendritic growth pattern of branches on (111) facets in <211> directions with the angle of 60° to the main trunk. [13, 60, 62, 74] When a trace Ag^+ (25 µM) was added, Figure 4-12B, the dendritic branches were shorter and almost disappeared. The SEM image

suggests that trace Ag^+ altered the growth pathway of gold microstructures by preventing the proliferation of the branch structures.
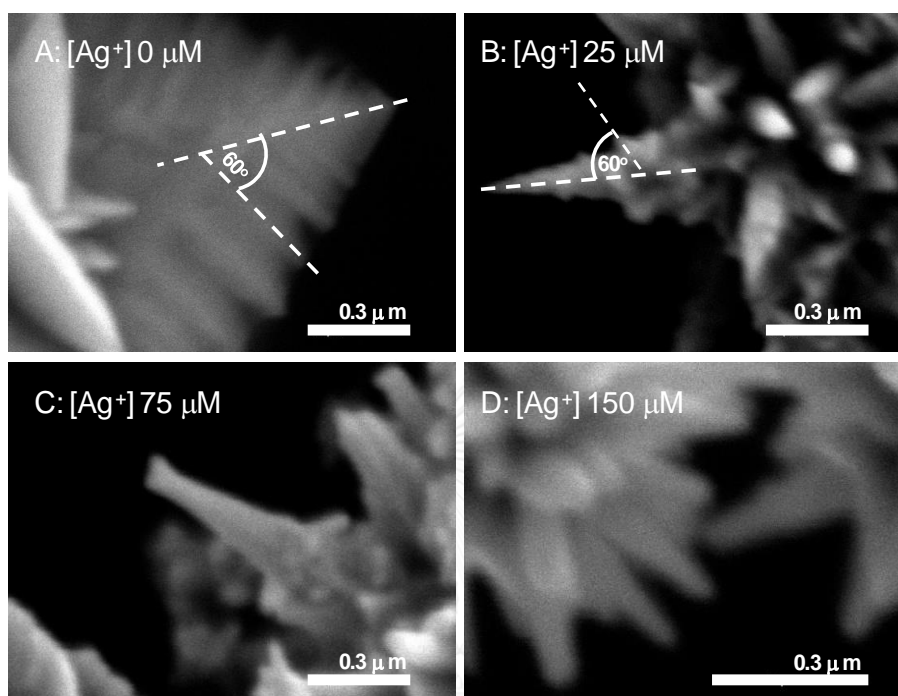
Figure 4-12   SEM images of (A) nanopetals (without Ag^+) and nanothorns with (B) 25 µM, (C) 75 µM, and (D) 150 µM Ag^+. The samples were collected after a 100-s reaction time. The concentrations of Au^{3+} and H_2O_2 were kept constant at 0.5 mM and 9 M, respectively. The scale bars indicate 0.3 µm.

When Ag^+ concentrations were increased to 75 µM (Figure 4-12C) and 150 µM (Figure 4-12D), the branches were completely disappeared while the trunks were substantially shortened. As the concentration of Ag^+ was further increased, the particle size became smaller and thorn length was shorter (Figure 4-6 and Table 4-1).When the concentration of Ag^+ was extremely high (300 µM, Figure 4-6I), the thorns were almost disappeared. The observed phenomena confirmed the role of physically adsorbed AgCl

on inhibiting dendritic growth by preventing the aggregated attachment of AuNPs on the branch structures.

To demonstrate idea about physical adsorption of metal chloride, lead ion (Pb^{2+}) was used for inducing solid lead chloride ($PbCl_2$) that compared with Ag^+ as shown in Figure 4-13. The results showed that Pb^{2+} could promote only FL-AuMSs and have ability to inhibit dendritic growth less than Ag^+ at the same loading. We assumed that solubility of AgCl and $PbCl_2$ played an importance role on controlling the development and growth of the nanothorn structures as shown in equation Eqs. 3-5 and 3-6:

$$Ag^+_{(aq)} + Cl^-_{(aq)} \rightleftharpoons AgCl_{(s)} \qquad K_{sp} = 1.8 \times 10^{-10} \qquad \text{(Eq. 3-5)}$$

$$Pb^{2+}_{(aq)} + 2Cl^-_{(aq)} \rightleftharpoons PbCl_{2(s)} \qquad K_{sp} = 5.89 \times 10^{-5} \qquad \text{(Eq. 3-5)}$$

The solubility products (K_{sp}) of AgCl and $PbCl_2$ suggest that AgCl could change to solid form at lower concentration than $PbCl_2$ due to the lower K_{sp}. Therefore, Ag^+ is converted into solid AgCl that could inhibit dendritic growth but Pb^{2+} cannot.
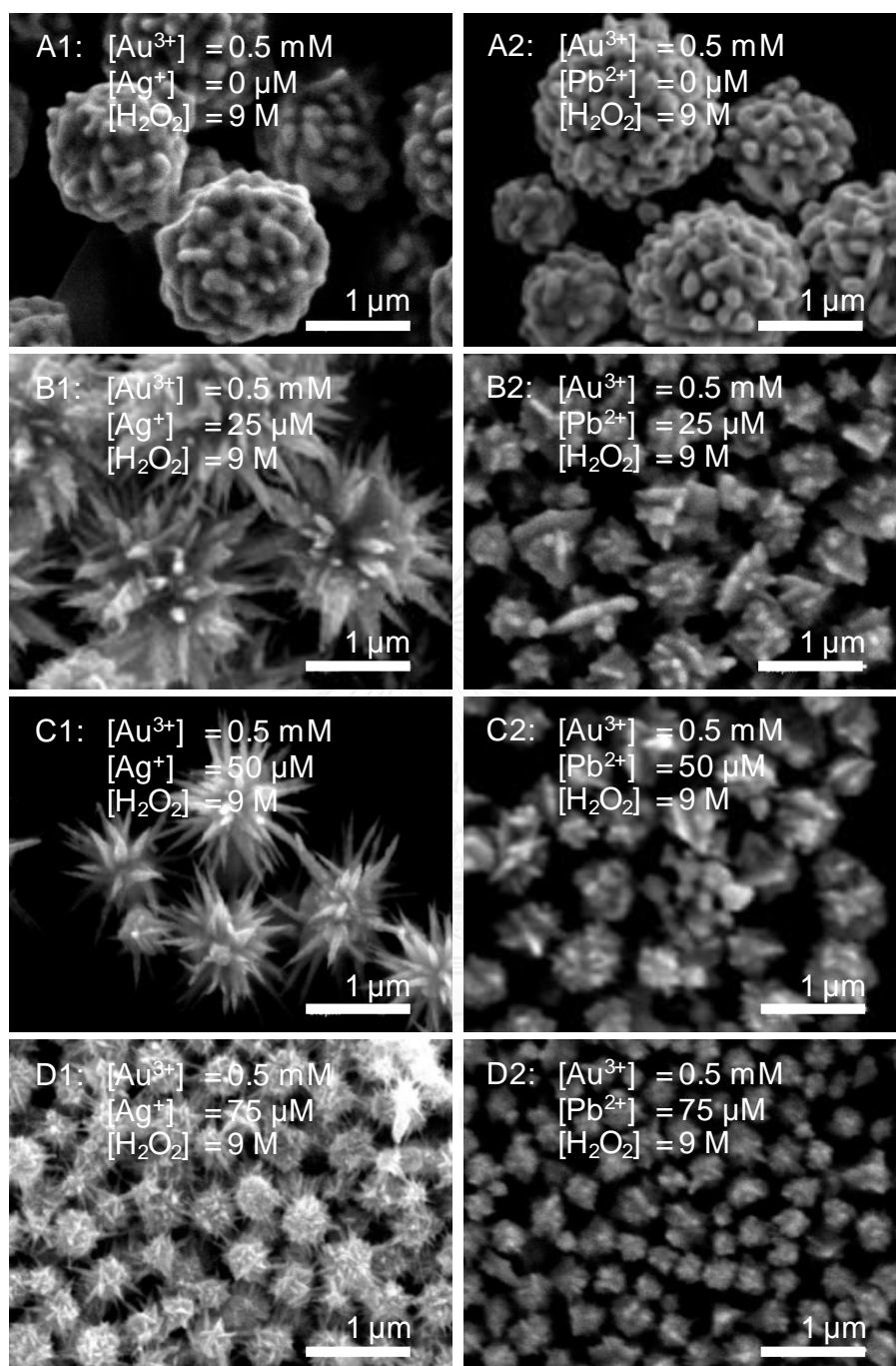
Figure 4-13 SEM images show variation of gold microstructures at various concentrations of Ag^+ and Pb^{2+} under a fixed concentration of Au^{3+} and H_2O_2 (0.5 mM and 9 M). The reaction ingredients are shown in the figures. Scale bars indicate 1 μm.

We proposed the formation and growth mechanism of QS-AuMSs and UL-AuMSs as shown in Scheme 4-1. A trace Ag^+ alters the growth of dendritic structures as it forms solid AgCl particles physically adsorbed onto gold surfaces and limited crystal growth in <211> direction. At a low concentration of Ag^+ (25 μM), the growth of branches was inhibited while the trunks grew into long nanothorns. A higher concentration of Ag^+ (50–150 μM) suppressed the growth of both branches and trunks while UL-AuMSs with shorter nanothorns were obtained. At a relatively high concentration of Ag^+ (greater than 200 μM), gold microstructure with small buds were obtained.
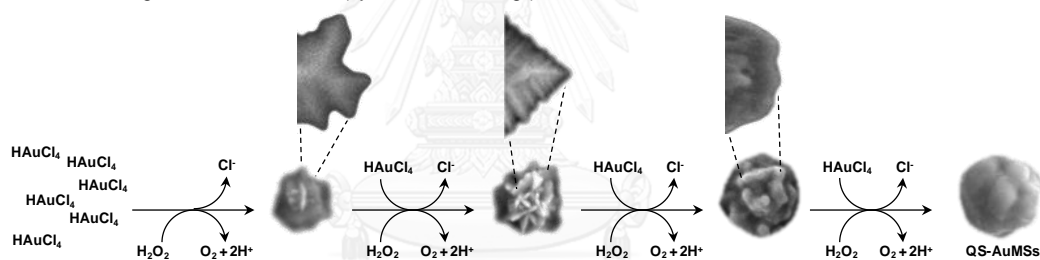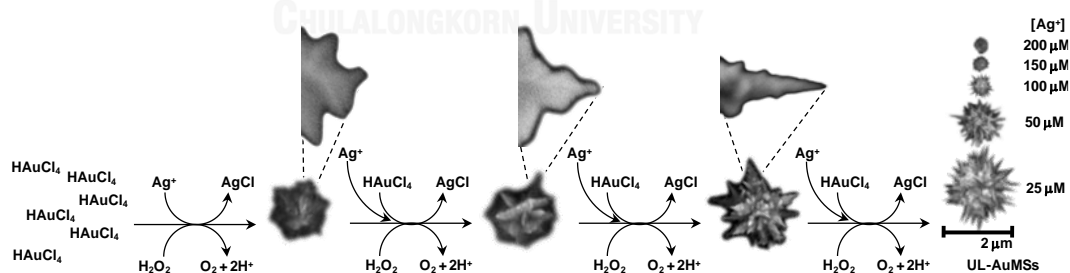
Scheme 4-1   Proposed growth mechanisms of (A) QS-AuMSs and (B) UL-AuMSs. Both QS-AuMSs and UL-AuMSs developed from FL-AuMSs.

4.4   The influences of pH on UL-AuMSs

The reduction efficiency of H_2O_2 is strongly depended on pH which is under acidic and alkaline conditions as shown in Eqs. 3-7 and 3-8, respectively.

$$H_2O_2 \rightarrow O_2 + 2H^+ + 2e^- \qquad\qquad E^o_{ox} = -0.695 \text{ V} \qquad\qquad \text{(Eq. 3-7)}$$

$$H_2O_2 + 2OH^- \rightarrow O_2 + 2H_2O + 2e^- \qquad\qquad E^o_{ox} = -0.146 \text{ V} \qquad\qquad \text{(Eq. 3-8)}$$
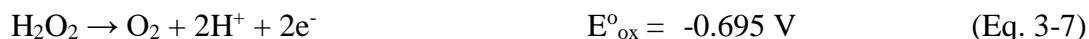
The reduction efficiency of H_2O_2 has directly affected on dendritic growth of UL-AuMSs which favors the weak reducing environment system under a kinetically control condition. [19] In this work, pH of H_2O_2 was adjusted by adding 0.1 M HNO_3 for acidic condition and 0.1 M NaOH for alkaline conditions. The final pH of H_2O_2 was ~1 and 9 after adding HCl and NaOH.

The large gold microplates were generated under the acidic condition (pH 1) as shown in Figure 4-14A1 and A2. Normally, 9 M H_2O_2 have pH ~5 that is suitable pH for producing QS-AuMSs and UL-AuMSs as shown in Figure 4-14B1 and B2. The results suggest that acidic condition of H_2O_2 promotes the growth more than the nucleation [53, 61] due to the low reduction efficiency of H_2O_2 under acidic environment. [66, 67] However, the size and surface morphology of gold microplates with Ag^+ (Figure 4-14A2) show the smaller size and smoother surface than those without Ag^+ (Figure 4-14A1) because of physical absorption and surface protection of AgCl on gold surface. [17, 18] At high alkaline condition (pH ~9), gold and silver nanoparticles could be generated by reduction of H_2O_2 as shown in Figure 4-14C1 and C2. [63, 67] In this work, without Ag^+, the spherical gold nanoparticles with the size of 30–50 nm and red colloid were obtained (Figure 4-14C1).
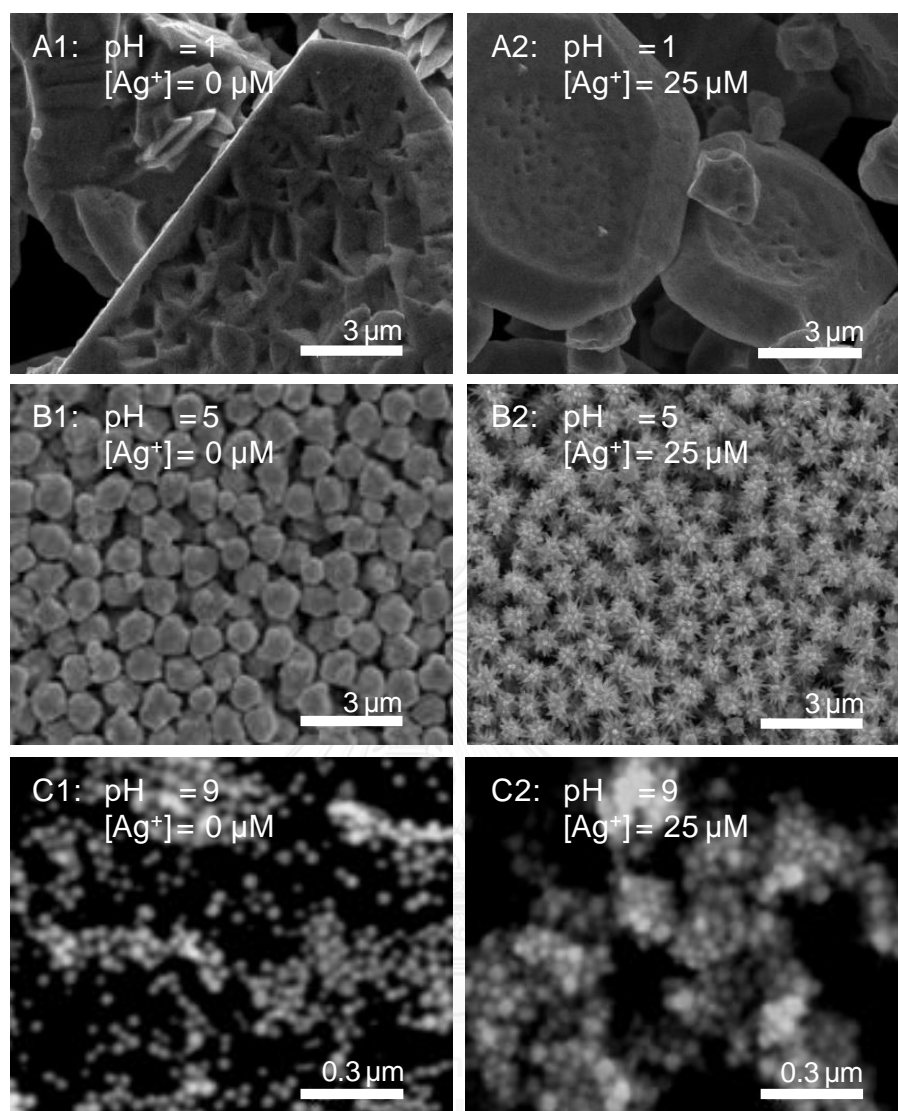
Figure 4-14 SEM images of gold microstructure with and without Ag^+ (25 μM) at difference pH: (A) pH 1, (B) pH 5, and (C) pH 9. The concentrations of Au^{3+} and H_2O_2 were kept constant at 0.5 mM and 9 M, respectively.

The spherical shape and small particles were controlled by thermodynamic control under high reducing efficiency [53, 61]. However, with Ag^+, spherical particles of 50–80 nm were synthesized (Figure 4-14C2) while large number of bubbles were released from colloid with red color (data not shown). These phenomena confirm the presence of gold nanoparticles and silver nanoparticles by the observation of red color

from plasmonic light absorption of gold nanoparticles and O_2 form catalytic decomposition of H_2O_2 on silver nanoparticles. [63, 67] The reaction at high alkaline condition (pH > 9) had been avoided due to high exothermic and possible explosion due to alkaline decomposition of H_2O_2.

4.5 The influences of Cl^- and NO_3^- on UL-AuMSs

The chloride ions (Cl^-) and nitrate ion (NO_3^-) are counter-ions from $HAuCl_4$ and $AgNO_3$. To observe the effect of these ions, adding Cl^- from NaCl and NO_3^- from $NaNO_3$ were investigated. At low concentrations (10 μM–1000 μM), both ions could not effect on growth pattern of UL-AuMSs and QS-AuMSs (data not shown). However, a high concentration of 0.1 M Cl^- (Figure 4-15B1 and B2) induced FL-AuMSs by Cl^- adsorption on gold surface. [75, 76] On the other hand, 0.1 M NO_3^- (Figure 4-15C1 and C2) shows insignificant effect on QS-AuMSs and UL-AuMSs because of low ability NO_3^- adsorption on gold surface. [77, 78]

4.6 The influences of temperature on UL-AuMSs

The reaction temperatures were observed at 20°, 28° (room temperature), and 40° C. The results suggest that the variation of temperature shows insignificant effect on structural changing of QS-AuMSs and UL-AuMSs from without and with Ag^+ in systems (Figure 4-16). However, the decrease of particle sizes both QS-AuMSs and UL-AuMSs were observed when temperature was increased. These results can be explained by free energy of nucleation step. [61] The low temperature can reduce free energy in system that prolongs the completed reduction time. Therefore, slower nucleation and growth induced the formation of larger particles.
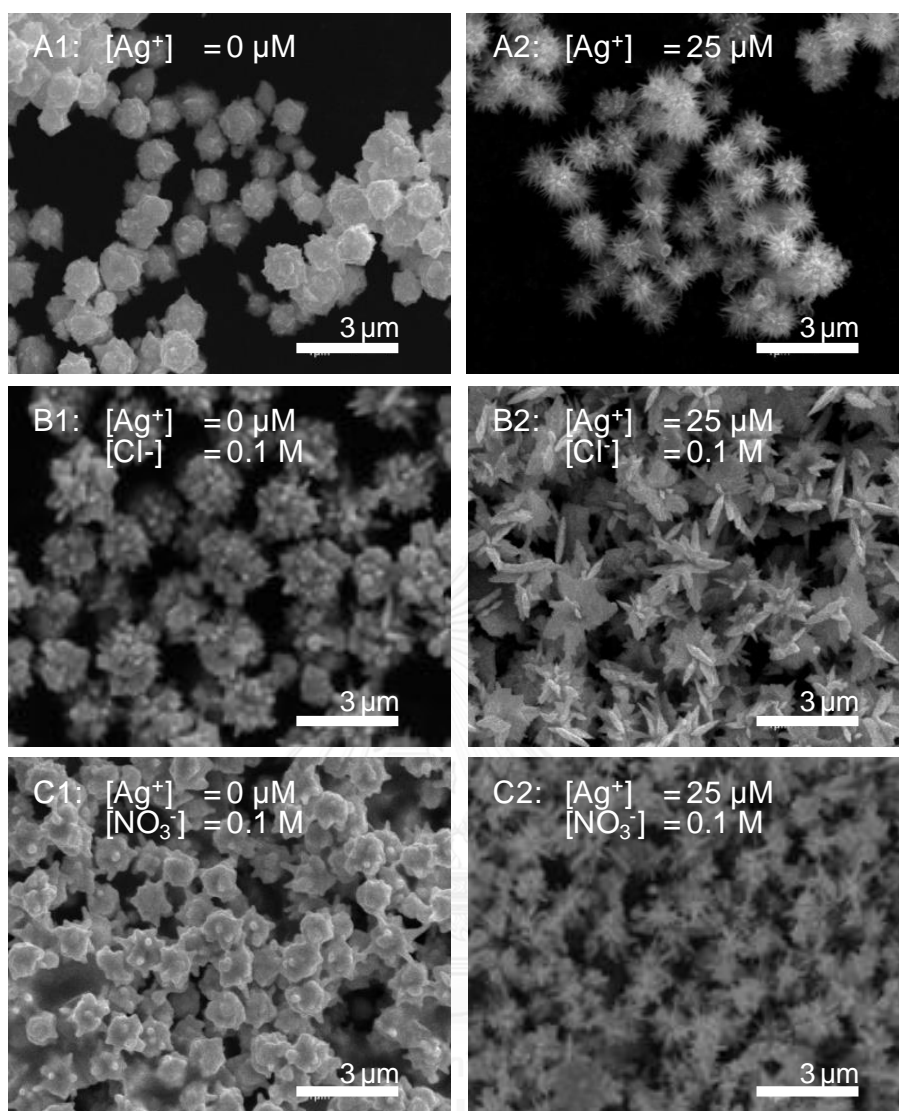
Figure 4-15 SEM images of gold microstructure with and without Ag^+ (25 μM) at difference counter-ion types: (A) without added counter-ions, (B) added Cl^-, and (C) added NO_3^-. The concentrations of Au^{3+} and H_2O_2 were kept constant at 0.5 mM and 9 M, respectively. The scale bars indicate 3 μm.
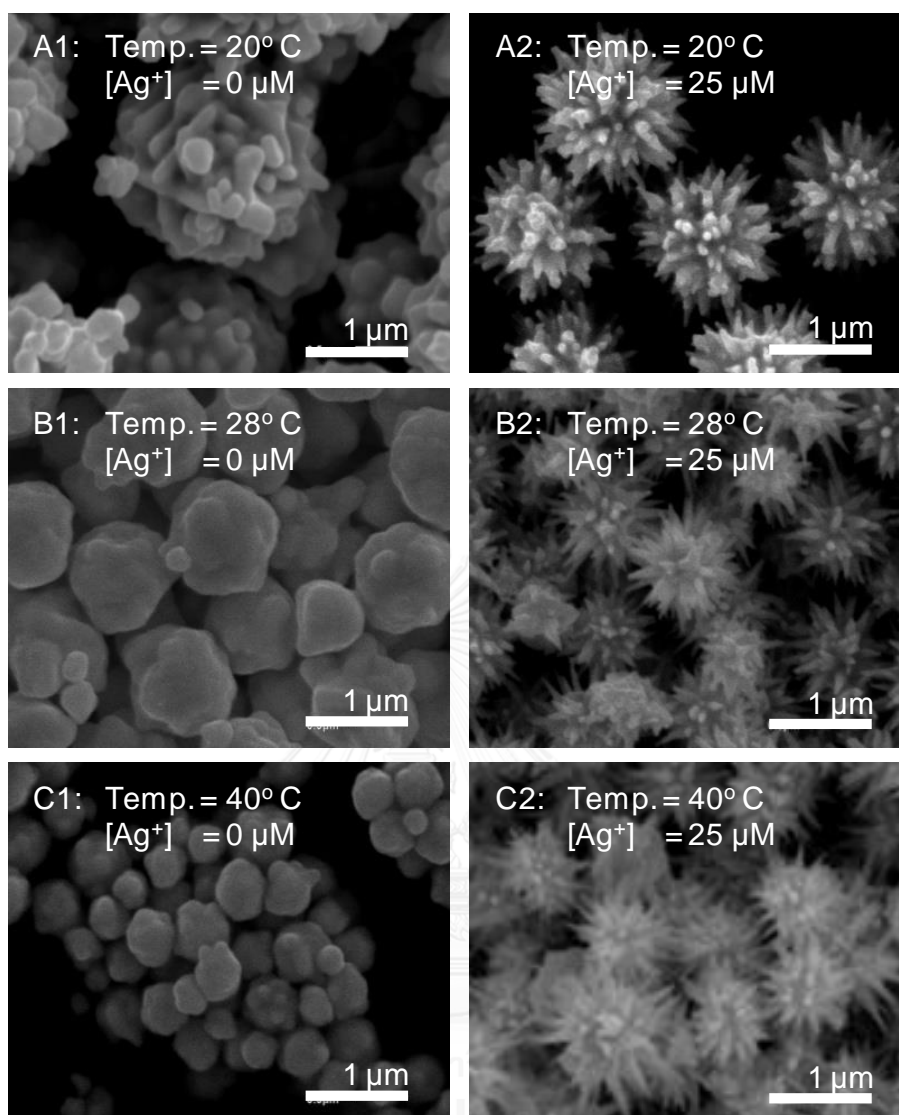
Figure 4-16   SEM images of gold microstructure with and without Ag$^+$ (25 µM) at difference temperature: (A) 20°, (B) 28°, and (C) 40° C. The concentrations of Au^{3+} and H$_2$O$_2$ were kept constant at 0.5 mM and 9 M, respectively. The scale bars indicate 1 µm.

4.7 SERS application

The synthesized UL-AuMSs could be employed as an efficient SERS substrate since they contain numerous sharp tips and narrow voids between nanothorns. As shown in Figure 4-6, a film of assembled UL-AuMSs contains additional voids and narrow gaps due to the intertwined nanothorns. The assembled UL-AuMSs should contain large number of hot spots with substantial SERS enhancement. [60, 79-81] To make an SERS substrate from UL-AuMSs, the residual AgCl film was removed by dissolving in NH_4OH solution. The AgCl-free UL-AuMSs was incubated in 1 µM R6G for 15 min before thoroughly rinsing with DI water to remove the un-immobilized R6G. The R6G-immobilized UL-AuMSs were assembled into a monolayer film on an aluminum substrate before acquiring SERS spectra, as shown Figure 4-17. Surprisingly, UL-AuMSs with the longest thorn length do not give the highest SERS signal (Figure 4-6B). The UL-AuMSs with very long thorns (Figure 4-6B (708 nm), 6C (638 nm), and 6D (288 nm)) and short thorns (Figure 4-6G (99 nm), 6H (60 nm), and 6I (32 nm)) gave SERS signal of the same magnitude as the QS-AuMSs (Figure 4-6A). UL-AuMSs with moderate thorn lengths shown in Figure 4-6E (187 nm) and 6F (166 nm), on the other hand, provided the highest SERS signals.

According to SEM images shown in Figure 4-6, inter-particle distances of UL-AuMSs did not play any role on the SERS enhancement since those with short distance (Figure 4-6G–I) gave the same signal as those with long distance (Figure 4-6B–D). Moreover, the intertwined thorns did not show any significant improvement since UL-AuMSs with long thorns (Figure 4-6B–D) gave smaller SERS enhancement than that of shorter thorns (Figure 4-6E and 6F).
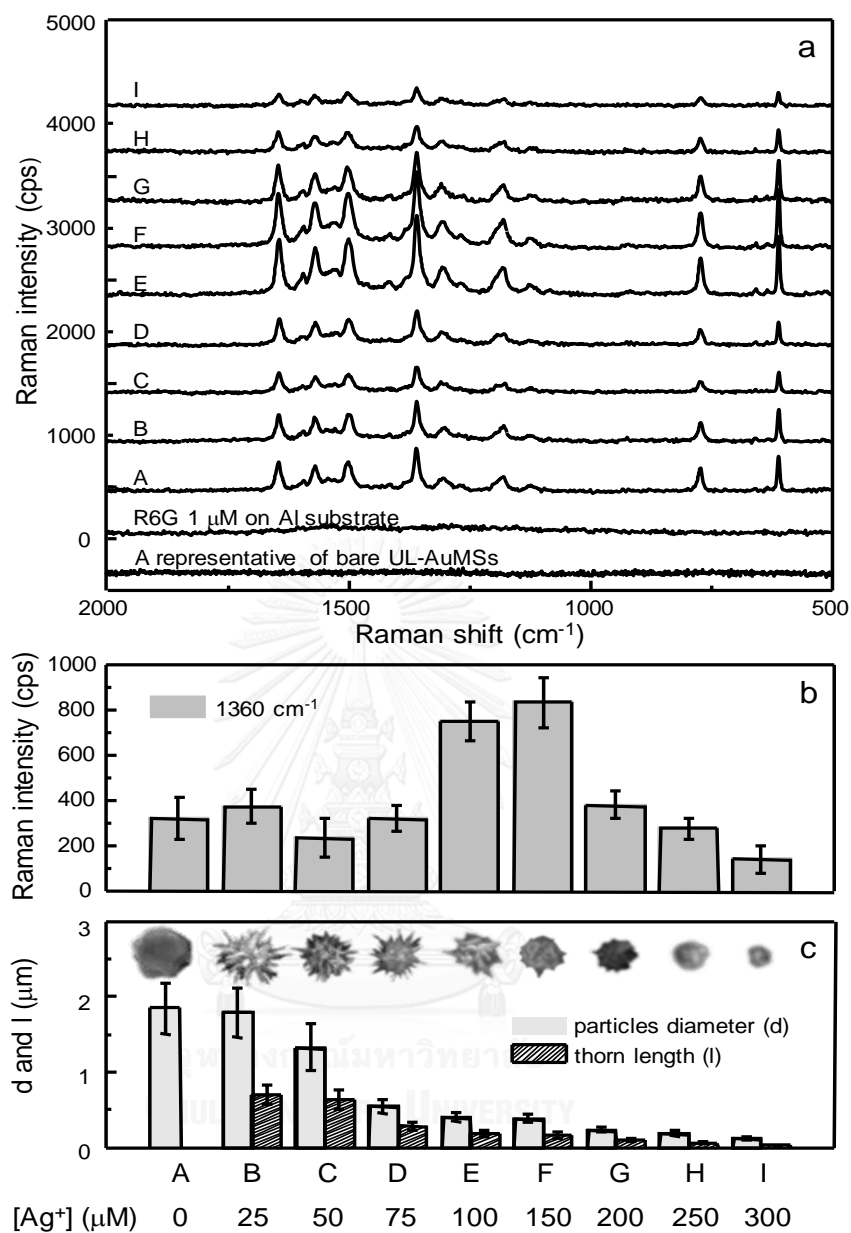
Figure 4-17 (a) SERS spectra of R6G (1 μM) immobilized on UL-AuMSs. (b) SERS

signals at 1360 cm^{-1} (C-C aromatic stretching) of immobilized R6G. (c)

Particle diameters and thorn lengths of UL-AuMSs obtained at various

Ag$^+$ concentrations. The results with QS-AuMSs ([Ag$^+$] = 0 μM) under

the same condition were added for comparison. All bare UL-AuMSs

substrates do not give any SERS signal. A–I represent QS-AuMSs and

UL-AuMSs shown in Figure 4-6 and Table 4-1.

Although the particle sizes were relatively large compared to those of nanospheres in previous reports, [82, 83] the enhancement of the UL-AuMSs originated from their surface morphologies containing thorns of optimal size and shape. The thorn length of 187 nm and 166 nm seem to provide the suitable conditions for the formation of hot spots (*i.e.*, thorn length, thorn sharpness, and inter-thorn gaps). [60, 79-81] Smaller UL-AuMSs (Figure4-6G–I) had thorns of decreased sharpness and less inter-thorn gaps (Figure 4-18). A high SERS enhancement of our UL-AuMSs was realized when it was employed as a substrate for trace R6G in water. The Raman band assignments of R6G showe in Table 4-2. [84] With rapid 15-min incubation in an analyte before a thorough rinsing, a relatively low concentration of 0.1 nM R6G can be detected (Figure 4-19).
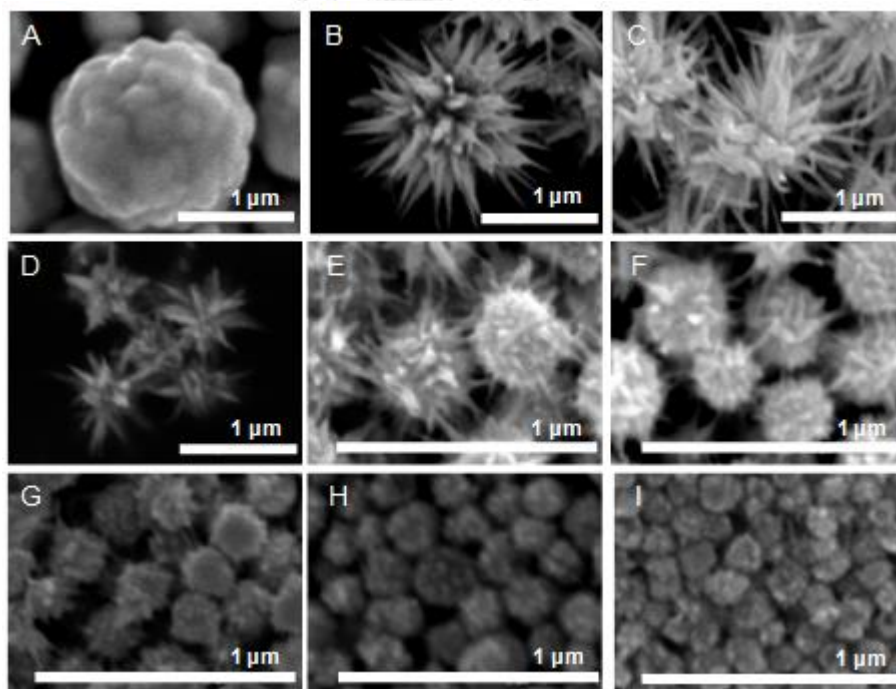
Figure 4-18   Enlarged SEM images of the inserts in Figure 4-6.

Table 4-2   Raman band assignments of R6G. [84]

Raman shift (cm^{-1})	Assignment
1652	
1600	
1575	C-C aromatic stressing
1446	
1360	
1312	
1187	C-H in-plane bending
776	C-H out-of-plane bending
662	C-C-C ring in-plane bending
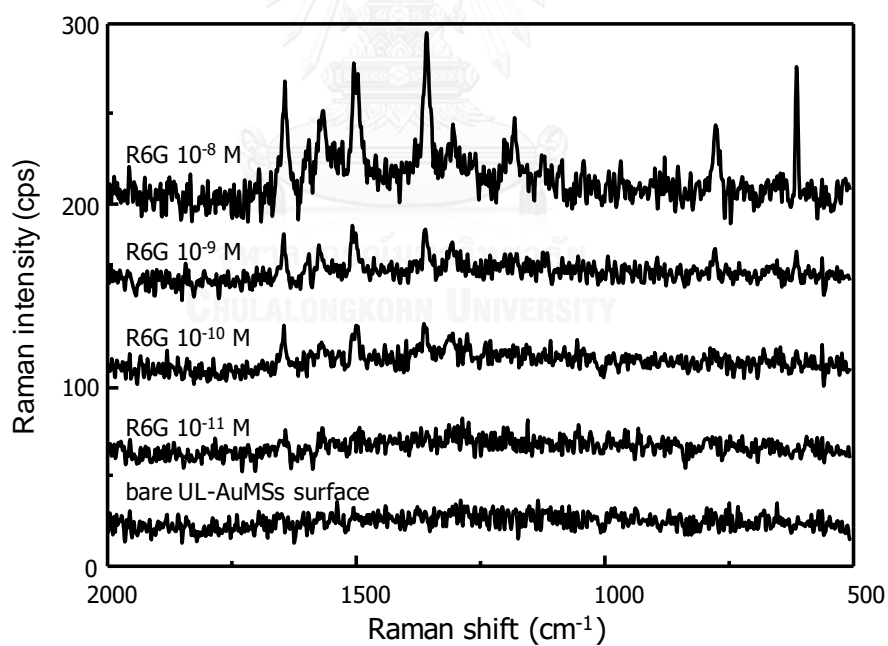
Figure 4-19   SERS spectra show the detectable concentration of R6G lowest at 0.1 nM using UL-AuMSs with thorn length of 166 nm as SERS substrates (Figure 4-6F).

One of the unique advantages of the micrometer size UL-AuMSs was their easy observation under an optical microscope. Figure 4-20 shows a cluster of UL-AuMSs on a gold microplate with ~20 μm lateral size. [52] The UL-AuMSs were immobilized with 1 μM R6G before deposition on the gold microplate. A dark spot of UL-AuMSs cluster against the shiny gold nanoplate can be distinctively detected under a 100x objective of a Raman microscope (Figure 4-20A). As a result, SERS specturm of the cluster can be selectively measured. Figure 4-20B shows SERS Raman map of the signal at 1360 cm^{-1} over the entire gold microplate. The map was constructed from 10×10 measured spots as shown by the grid in Figure 4-20A. The highest SERS singal representing R6G coincided with the center of the UL-AuMSs cluster (Figure 4-20B). Figure 4-20C shows SERS spectra along the line-map across the center of the cluster. The R6G singnal decreased as the measured spot drift away from the center of the cluster (spots No. 1 and 3).
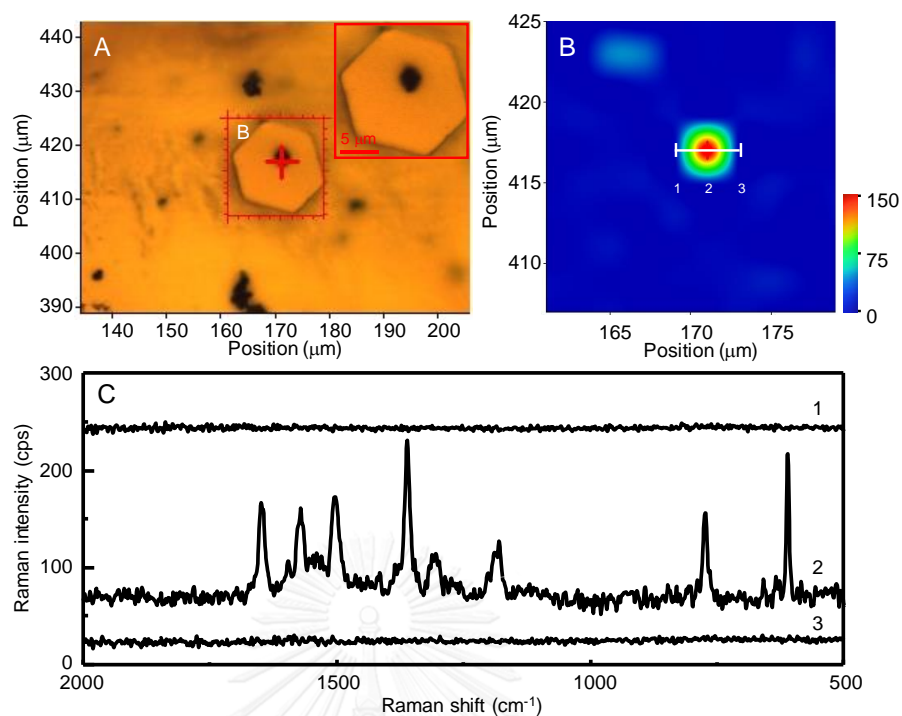
Figure 4-20 (A) An optical microscope image of a cluster of UL-AuMSs on a gold microplate captured through a 100x objective. (B) Raman map with SERS signals of R6G at 1360 cm^{-1} with a 2 μm step. The map contained 10×10 measured spots with color scale representing SERS intensity (cps). (C) SERS spectra represent a line map of 3-measured spots across the center of UL-AuMSs cluster shown (B).

4.8   Hemi-spherical gold microstructures

In this work, without Ag^+, hemi spherical gold microstructures (HS-AuMSs) are minor product when QS-AuMSs were synthesized as shown in Figure 4-21. The high concentrations of Au^{3+} (from 5 to 10 mM) were suitable for produce high quantity of HS-AuMSs. The particles sizes of HS-AuMSs were 2–10 μm. FL-AuMSs appeared when silver ions were added in system with increasing concentrations of gold ions (Figure 4-3). We hypothesized that one possible mechanism to control the growth of HS-AuMSs is physical suppression on flat surface of hemispherical shape. To confirm our hypothesis, an experimental design was set as shown in Figure 3-2 to observe the physical suppression on HS-AuMSs.

The samples collected from position A–D on mica sheet (Figure 3-2) were investigated, as shown in Figure 4-22. The gold microplates with the sizes of 0.3–0.8 μm were sampling from position A as shown in Figure 4-22A. HS-AuMSs with the sizes of 1.5–2 μm were collected from positions B and C as shown in Figure 4-22B and 4-22C, respectively. Incomplete QS-AuMSs with the sizes around 2 μm were collected form position D as shown in Figure 4-22D. These results suggest that different distance from surface of mixture solution to mica sheet plays the important role to induce the formation of HS-AuMSs. The short distance (position A, B and C) could induce fast deposition of particles in early stage of growth period. The attachment of particles on substrate can protect one size from particles growth in mixture solution. Therefore, we could observe HS-AuMSs as minor product mixing QS-AuMSs as major product.
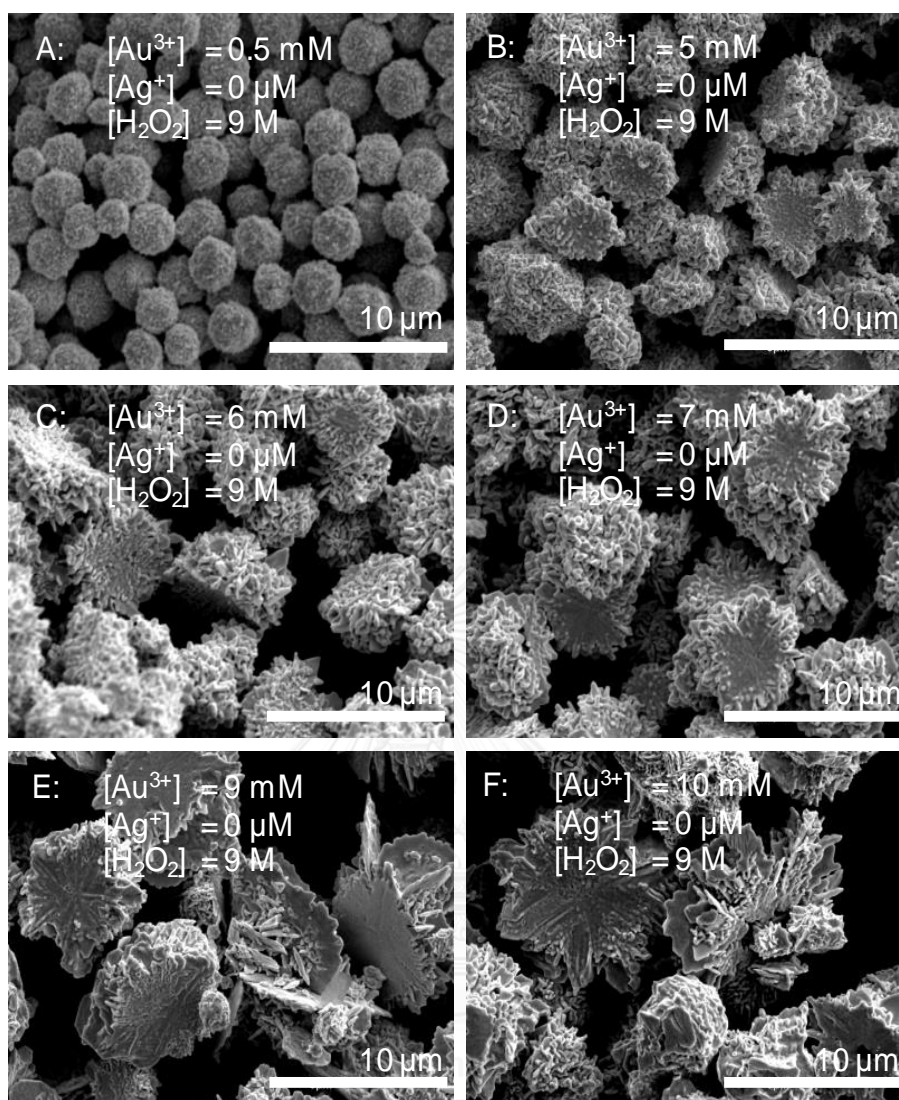
Figure 4-21 SEM images show the increasing of particle sizes of HS-AuMSs as the concentrations of Au^{3+} were increased: (A) 0.5, (B) 5, (C) 6, (D) 7, (E) 9, and (F) 100 mM. The concentration of H_2O_2 was kept constant at 9 M, respectively. The insets show enlarged images. Scale bars indicate 10 μm.
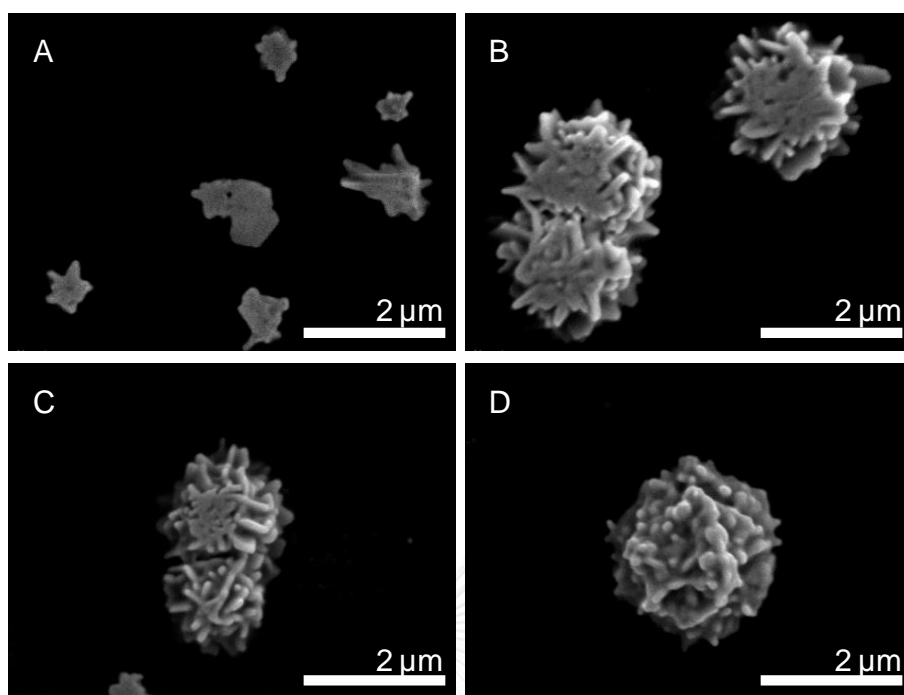
Figure 4-22 SEM images show the variation of shape (A) gold microplates, (B and C) HS-AuMSs and (D) Incomplete QS-AuMSs. The concentration of Au^{3+} and H_2O_2 were kept constant at 5 and 9 M, respectively. Scale bars indicate 2 μm.

4.9 Urchin-like gold nanoparticles

In section 4.3, the role of silver ions to induce the formation of nanothorns on UL-AuMSs was explored. By seed-mediated growth, rate of nucleation was increase when gold nanoparticles were added as seed particles during the reduction process. [7] Therefore, particles size of UL-AuMSs in micro-scale will be decreased to nano-scale when seed particles were introduced. We demonstrated that we could use a seed-mediated growth for synthesizing urchin-like gold nanoparticles (UL-AuNPs) as shown in TEM image, Figure 4-23B (*i.e.,* the white-covered layer on UL-AuMSs came from retaining moisture on particles). The particles sizes of UL-AuNPs were 60-80 nm with

gold nanothorns of 10-30 nm. UL-AuNPs showed the broadband of light absorption

from 500–800 nm, as shown in Figure 4-23D, which can apply for light-harvesting or

nanoantenna in plasmonic solar cells [7] and plasmonic heating. [85]
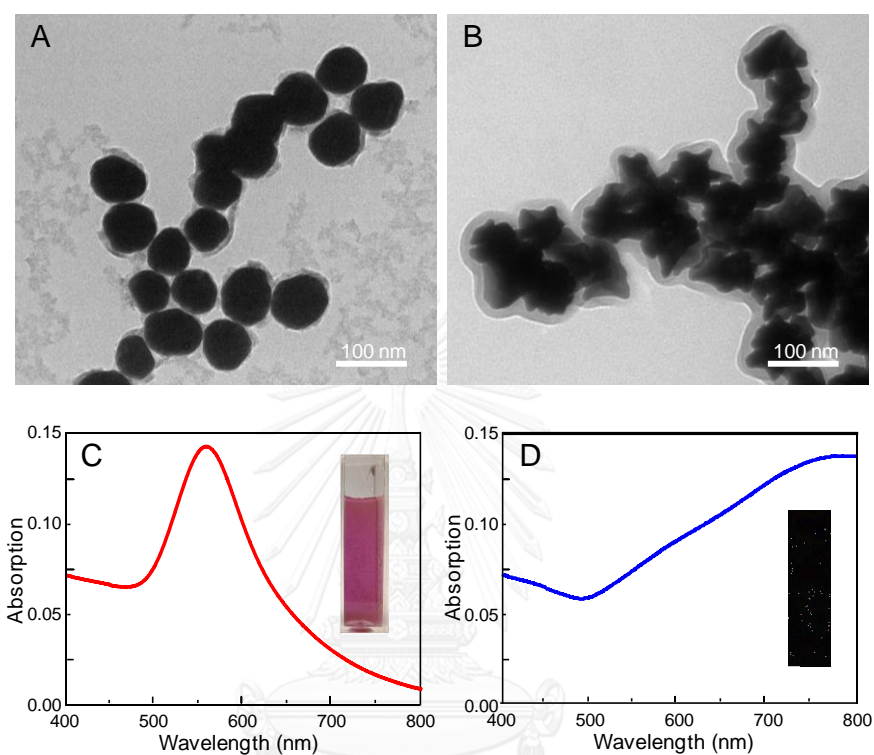
Figure 4-23   TEM images show (A) spherical gold nanoparticles and (B) UL-AuNPs

from without and with 25 μM Ag^+ under seed-mediated growth. Scale

bars indicate 100 nm. UV-Visible absorption spectra with insert digital

images show characteristic of (C) spherical gold nanoparticles and UL-

AuNPs, respectively. The concentration of Au^{3+} and H_2O_2 were kept

constant at 5 and 9 M, respectively.

CHAPTER V
CONCLUSIONS

We have successfully synthesized complex gold micro/nanostructures as UL-AuMSs with controllable length of nanothorns *via* a simple one-pot synthetic protocol consisting of Au^{3+}, H_2O_2, and trace Ag^+. We also verified the governing mechanism of trace Ag^+ on the formation and growth of nanothorns. The presence of trace Ag^+ is necessary for the nanothorn formation. Without Ag^+, QS-AuMSs were the sole product. By taking advantage of the selectively surface passivation of Cl^- on Au (111), an addition of trace Ag^+ with a concomitant formation of solid AgCl capable of suppressing the growth of dendritic structures enabled a control of thorn length. At a low concentration of Ag^+ (25 μM), the growth of branches was inhibited while the trunks grew into long nanothorns. However, a higher concentration of Ag^+ (50–150 μM) suppressed the growth of both branches and trunks and UL-AuMS with short nanothorns were obtained. The UL-AuMSs with thorn length of 166 and 187 nm show high SERS enhancement as they possessed optimal thorn lengths, thorn sharpness and inter-thorn gaps for the formation of hot spots. A low concentration of 0.1 nM R6G could be detected with a short 15-min incubation. The micrometer size UL-AuMSs with efficient hot spot can be exploited for location specific SERS measurement.

Not only effect of Au^{3+}, H_2O_2, and trace Ag^+ concentrations on complex gold micro/nanostructures were investigated, but also other parameters such as pH, counter ions (Cl^- and NO_3^-) and temperature were explored. We found that these parameters have effect on structure and size of complex gold micro/nanostructures. Moreover, we have successfully explained the growth mechanism of hemi-spherical gold

microstructures (HS-AuMSs) due to deposition of particles on a flat mica surface at the early stage of growth period. Furthermore, we have successfully synthesized urchin-like gold nanoparticles (UL-AuNPs) by seed-mediated growth. The obtained UL-AuNPs showed high potential applications is plasmonic solar cells and plasmonic heating.

REFERENCES

1. Du, X.; Zhang, Z.; Miao, Z.; Ma, M.; Zhang, Y.; Zhang, C.; Wang, W.; Han, B.; Chen, Q., One step electrodeposition of dendritic gold nanostructures on β-lactoglobulin-functionalized reduced graphene oxide for glucose sensing. *Talanta* **2015**, 144, 823–829.

2. Dehdari Vais, R.; Sattarahmady, N.; Karimian, K.; Heli, H., Green electrodeposition of gold hierarchical dendrites of pyramidal nanoparticles and determination of azathioprine. *Sens. Actuators B Chem.* **2015**, 215, 113–118.

3. Xia, T.; Luo, H.; Wang, S.; Liu, J.; Yu, G.; Wang, R., Large-scale synthesis of gold dendritic nanostructures for surface enhanced Raman scattering. *CrystEngComm* **2015**, 17 (22), 4200–4204.

4. Niu, W.; Chua, Y. A. A.; Zhang, W.; Huang, H.; Lu, X., Highly symmetric gold nanostars: crystallographic control and surface-enhanced Raman scattering property. *J. Am. Chem. Soc.* **2015**, 137 (33), 10460–10463.

5. Cui, Q.; Xia, B.; Mitzscherling, S.; Masic, A.; Li, L.; Bargheer, M.; Möhwald, H., Preparation of gold nanostars and their study in selective catalytic reactions. *Colloids Surf., A* **2015**, 465, 20–25.

6. Nguyen, A. H.; Ma, X.; Sim, S. J., Gold nanostar based biosensor detects epigenetic alterations on promoter of real cells. *Biosens. Bioelectron.* **2015**, 66, 497–503.

7. Pangdam, A.; Nootchanat, S.; Ishikawa, R.; Shinbo, K.; Kato, K.; Kaneko, F.; Thammacharoen, C.; Ekgasit, S.; Baba, A., Effect of urchin-like gold

nanoparticles in organic thin-film solar cells. *Phys. Chem. Chem. Phys.* **2016**, 18, 18500–18506.

8. Ren, W.; Huang, Z.; Xu, Y.; Li, Y.; Ji, Y.; Su, B., Urchin-like gold nanoparticle-based immunochromatographic strip test for rapid detection of fumonisin B1 in grains. *Anal. Bioanal. Chem.* **2015**, 407 (24), 7341–7348.

9. Sabri, Y. M.; Kandjani, A. E.; Ippolito, S. J.; Bhargava, S. K., Ordered monolayer gold nano-urchin structures and their size induced control for high gas sensing performance. *Sci. Rep.* **2016**, 6.

10. Plascencia-Villa, G. n.; Torrente, D.; Marucho, M.; José-Yacamán, M., Biodirected synthesis and nanostructural characterization of anisotropic gold nanoparticles. *Langmuir* **2015**, 31 (11), 3527–3536.

11. Hao, E.; Bailey, R. C.; Schatz, G. C.; Hupp, J. T.; Li, S., Synthesis and optical properties of "branched" gold nanocrystals. *Nano Lett.* **2004**, 4 (2), 327–330.

12. Hao, F.; Nehl, C. L.; Hafner, J. H.; Nordlander, P., Plasmon resonances of a gold nanostar. *Nano Lett.* **2007**, 7 (3), 729–732.

13. Huang, D.; Qi, Y.; Bai, X.; Shi, L.; Jia, H.; Zhang, D.; Zheng, L., One-pot synthesis of dendritic gold nanostructures in aqueous solutions of quaternary ammonium cationic surfactants: effects of the head group and hydrocarbon chain length. *ACS Appl. Mater. Interfaces* **2012**, 4 (9), 4665–4671.

14. Khoury, C. G.; Vo-Dinh, T., Gold nanostars for surface-enhanced Raman scattering: synthesis, characterization and optimization. *J. Phys. Chem. C* **2008**, 112 (48), 18849–18859.

15. Garcia-Leis, A.; Torreggiani, A.; Garcia-Ramos, J. V.; Sanchez-Cortes, S., Hollow Au/Ag nanostars displaying broad plasmonic resonance and high surface-enhanced Raman sensitivity. *Nanoscale* **2015**, 7 (32), 13629–13637.

16. Jana, S. K.; Saha, B.; Satpati, B.; Banerjee, S., Structural and electrochemical analysis of a novel co-electrodeposited Mn_2O_3-Au nanocomposite thin film. *Dalton Trans.* **2015**, 44 (19), 9158–9169.

17. Yuan, H.; Ma, W.; Chen, C.; Zhao, J.; Liu, J.; Zhu, H.; Gao, X., Shape and SPR evolution of thorny gold nanoparticles promoted by silver ions. *Chem. Mater.* **2007**, 19 (7), 1592–1600.

18. Yuan, H.; Ma, W.; Chen, C.; Zhu, H.; Gao, X.; Zhao, J., Controllable synthesis of 3D thorny plasmonic gold nanostructures and their tunable optical properties. *J. Phys. Chem. C* **2011**, 115 (47), 23256–23260.

19. Yuan, H.; Khoury, C. G.; Hwang, H.; Wilson, C. M.; Grant, G. A.; Vo-Dinh, T., Gold nanostars: surfactant-free synthesis, 3D modelling, and two-photon photoluminescence imaging. *Nanotechnology* **2012**, 23 (7), 075102.

20. Sajanlal, P.; Pradeep, T., Mesoflowers: A new class of highly efficient surface-enhanced Raman active and infrared-absorbing materials. *Nano Research* **2009**, 2 (4), 306–320.

21. Sanchez-Gaytan, B. L.; Swanglap, P.; Lamkin, T. J.; Hickey, R. J.; Fakhraai, Z.; Link, S.; Park, S. J., Spiky gold nanoshells: synthesis and enhanced scattering properties. *J. Phys. Chem. C* **2012**, 116 (18), 10318–10324.

22. Lopez-Serrano, A.; Olivas, R. M.; Landaluze, J. S.; Camara, C., Nanoparticles: a global vision characterization, separation, and quantification methods potential environmental and health impact. *Anal. Methods* **2014**, 6 (1), 38–56.

23.   Tsuzuki, T., Commercial scale production of inorganic nanoparticles. *Int. J. Nanotechnol.* **2009**, 6 (5-6), 567–578.

24.   Cantaert, B.; Ding, D.; Rieu, C.; Petrone, L.; Hoon, S.; Kock, K. H.; Miserez, A., Stable formation of gold nanoparticles onto redox-active solid biosubstrates made of squid suckerin proteins. *Macromol. Rapid Commun.* **2015**, 2015, 36 (21), 1877–1883.

25.   Kuo, C. H.; Li, W.; Pahalagedara, L.; El-Sawy, A. M.; Kriz, D.; Genz, N.; Guild, C.; Ressler, T.; Suib, S. L.; He, J., Understanding the role of gold nanoparticles in enhancing the catalytic activity of manganese oxides in water oxidation reactions. *Angew. Chem. Int. Ed.* **2015**, 54 (8), 2345–2350.

26.   Paul, B.; Bhuyan, B.; Purkayastha, D. D.; Dey, M.; Dhar, S. S., Green synthesis of gold nanoparticles using Pogestemon benghalensis (B) O. Ktz. leaf extract and studies of their photocatalytic activity in degradation of methylene blue. *Mater. Lett.* **2015**, 148, 37–40.

27.   Kamaliya, B.; Vijay Kumar, M.; Yelamaggad, C. V.; Krishna Prasad, S., Enhancement of electrical conductivity of a liquid crystal-gold nanoparticle composite by a gel network of aerosil particles. *Appl. Phys. Lett.* **2015**, 106 (8), 083110.

28.   Korotcenkov, G.; Brinzari, V.; Gulina, L. B.; Cho, B. K., The influence of gold nanoparticles on the conductivity response of SnO_2-based thin film gas sensors. *Appl. Surf. Sci.* **2015**, 353, 793–803.

29.   Fernandes, R.; Smyth, N. R.; Muskens, O. L.; Nitti, S.; Heuer-Jungemann, A.; Ardern-Jones, M. R.; Kanaras, A. G., Interactions of skin with gold

nanoparticles of different surface charge, shape, and functionality. *Small* **2015**, 11 (6), 713–721.

30.   MacLeod, M. J.; Johnson, J. A., PEGylated N-heterocyclic carbene anchors designed to stabilize gold nanoparticles in biologically relevant media. *J. Am. Chem. Soc.* **2015**, 137 (25), 7974–7977.

31.   Piella, J.; Bastús, N. G.; Puntes, V., Size-controlled synthesis of sub-10-nanometer citrate-stabilized gold nanoparticles and related optical properties. *Chem. Mater.* **2016**, 28 (4), 1066–1075.

32.   Sumi, T.; Motono, S.; Ishida, Y.; Shirahata, N.; Yonezawa, T., Formation and optical properties of fluorescent gold nanoparticles obtained by matrix sputtering method with volatile mercaptan molecules in the vacuum chamber and consideration of their structures. *Langmuir* **2015**, 31 (14), 4323–4329.

33.   Murphy, C. J.; Gole, A. M.; Hunyadi, S. E.; Stone, J. W.; Sisco, P. N.; Alkilany, A.; Kinard, B. E.; Hankins, P., Chemical sensing and imaging with metallic nanorods. *Chem. Commun.* **2008**, (5), 544–557.

34.   Das, S. K.; Das, A. R.; Guha, A. K., Microbial synthesis of multishaped gold nanostructures. *Small* **2010**, 6 (9), 1012–1021.

35.   Lermé, J., Size evolution of the surface plasmon resonance damping in silver nanoparticles: confinement and dielectric effects. *J. Phys. Chem. C* **2011**, 115 (29), 14098–14110.

36.   Kelly, K. L.; Coronado, E.; Zhao, L. L.; Schatz, G. C., The optical properties of metal nanoparticles: the influence of size, shape, and dielectric environment. *J. Phys. Chem. B* **2003**, 107 (3), 668–677.

37.   Zhou, Y.; Han, H.; Naw, H. P. P.; Lammy, A. V.; Goh, C. H.; Boujday, S.; Steele, T. W. J., Real-time colorimetric hydration sensor for sport activities. *Mat. Des.* **2016**, 90, 1181–1185.

38.   Kolemen, S.; Ozdemir, T.; Lee, D.; Kim, G. M.; Karatas, T.; Yoon, J.; Akkaya, E. U., Remote-controlled release of singlet oxygen by the plasmonic heating of endoperoxide-modified gold nanorods: towards a paradigm change in photodynamic therapy. *Angew. Chem. Int. Ed.* **2016**, 55 (11), 3606–3610.

39.   Sharma, M.; Pudasaini, P. R.; Ruiz-Zepeda, F.; Vinogradova, E.; Ayon, A. A., Plasmonic Effects of Au/Ag Bimetallic Multispiked Nanoparticles for Photovoltaic Applications. *ACS Appl. Mater. Interfaces* **2014**, 6 (17), 15472–15479.

40.   Zhao, H.; Jin, J.; Tian, W.; Li, R.; Yu, Z.; Song, W.; Cong, Q.; Zhao, B.; Ozaki, Y., Three-dimensional superhydrophobic surface-enhanced Raman spectroscopy substrate for sensitive detection of pollutants in real environments. *J. Mat. Chem. A* **2015**, 3 (8), 4330–4337.

41.   Guillot, N.; de la Chapelle, M. L., The electromagnetic effect in surface enhanced Raman scattering: Enhancement optimization using precisely controlled nanostructures. *J. Quant. Spectrosc. Radiat. Transfer* **2012**, 113 (18), 2321–2333.

42.   Ding, S. Y.; Yi, J.; Li, J.-F.; Ren, B.; Wu, D. Y.; Panneerselvam, R.; Tian, Z. Q., Nanostructure-based plasmon-enhanced Raman spectroscopy for surface analysis of materials. *Nat. Rev. Mater.* **2016**, 1, 16021.

43.   Birol, H.; Renato Rambo, C.; Guiotoku, M.; Hotza, D., Preparation of ceramic nanoparticles via cellulose-assisted glycine nitrate process: a review. *RSC Adv.* **2013**, 3 (9), 2873–2884.

44.   Toshima, N.; Yonezawa, T., Bimetallic nanoparticles-novel materials for chemical and physical applications. *New J. Chem.* **1998**, 22 (11), 1179–1201.

45.   Weisheng, Y.; Zhihong, W.; Yang, Y.; Longqing, C.; Ahad, S.; Kimchong, W.; Xianbin, W., Electron-beam lithography of gold nanostructures for surface-enhanced Raman scattering. *J Micromech. Microeng.* **2012**, 22 (12), 125007.

46.   Luo, X.; Du, L.; Wen, Z.; Lv, W.; Zhao, F.; Jiang, X.; Peng, Y.; Sun, L.; Li, Y.; Rao, J., Remarkably enhanced red-NIR broad spectral absorption via gold nanoparticles: applications for organic photosensitive diodes. *Nanoscale* **2015**, 7 (34), 14422–14433.

47.   Xu, X.; Duan, G.; Li, Y.; Liu, G.; Wang, J.; Zhang, H.; Dai, Z.; Cai, W., Fabrication of gold nanoparticles by laser ablation in liquid and their application for simultaneous electrochemical detection of Cd^{2+}, Pb^{2+}, Cu^{2+}, Hg^{2+}. *ACS Appl. Mater. Interfaces* **2014**, 6 (1), 65–71.

48.   Meng, F.; Morin, S. A.; Forticaux, A.; Jin, S., Screw dislocation driven growth of nanomaterials. *Acc. Chem. Res.* **2013**, 46 (7), 1616–1626.

49.   Li, Q.; Lu, B.; Zhang, L.; Lu, C., Synthesis and stability evaluation of size-controlled gold nanoparticles via nonionic fluorosurfactant-assisted hydrogen peroxide reduction. *J. Mater. Chem.* **2012**, 22 (27), 13564–13570.

50.   Gao, J.; Bender, C. M.; Murphy, C. J., Dependence of the gold nanorod aspect ratio on the nature of the directing surfactant in aqueous solution. *Langmuir* **2003**, 19 (21), 9065–9070.

51.   Schütz, M.; Steinigeweg, D.; Salehi, M.; Kömpe, K.; Schlücker, S.,
       Hydrophilically stabilized gold nanostars as SERS labels for tissue imaging of
       the tumor suppressor p63 by immuno-SERS microscopy. *Chem. Commun.*
       2011, 47 (14), 4216–4218.

52.   Nootchanat, S.; Thammacharoen, C.; Lohwongwatana, B.; Ekgasit, S.,
       Formation of large H_2O_2-reduced gold nanosheets via starch-induced two-
       dimensional oriented attachment. *RSC Adv.* **2013**, 3 (11), 3707–3716.

53.   Xia, Y.; Xiong, Y.; Lim, B.; Skrabalak, S. E., Shape-controlled synthesis of
       metal nanocrystals: simple chemistry meets complex physics? *Angew. Chem.*
       Int. Ed. **2009**, 48 (1), 60–103.

54.   Thanh, N. T. K.; Maclean, N.; Mahiddine, S., Mechanisms of nucleation and
       growth of nanoparticles in solution. *Chem. Rev.* **2014**, 114 (15), 7610–7630.

55.   Sun, Y., Interfaced heterogeneous nanodimers. *Natl. Sci. Rev.* **2015**, 2 (3), 329–
       348.

56.   Lee, L. J.; Zeng, C.; Cao, X.; Han, X.; Shen, J.; Xu, G., Polymer nanocomposite
       foams. *Compos. Sci. Technol.* **2005**, 65 (15), 2344–2363.

57.   Lv, W.; Zhu, Y.; Niu, Y.; Huo, W.; Li, K.; Zhu, G.; Liang, Y.; Wu, W.; He, W.,
       Assembly of anisotropic one dimensional Ag nanostructures through orientated
       attachment: on-axis or off-axis growth? *RSC Adv.* **2015**, 5 (27), 20783–20787.

58.   Penn, R. L.; Banfield, J. F., Morphology development and crystal growth in
       nanocrystalline aggregates under hydrothermal conditions: insights from titania.
       Geochim. Cosmochim. Acta **1999**, 63 (10), 1549–1557.

59.   Liu, X.; Xu, J.; Fang, Z.; Lin, L.; Qian, Y.; Wang, Y.; Ye, C.; Ma, C.; Zeng, J.,
        One-pot synthesis of Bi_2Se_3 nanostructures with rationally tunable
        morphologies. *Nano Res.* **2015,** 8 (11), 3612–3620.

60.   Huang, D.; Bai, X.; Zheng, L., Ultrafast preparation of three-dimensional
        dendritic gold nanostructures in aqueous solution and their applications in
        catalysis and SERS. *J. Phys. Chem. C* **2011**, 115 (30), 14641–14647.

61.   Xia, Y.; Xia, X.; Peng, H. C., Shape-controlled synthesis of colloidal metal
        nanocrystals: thermodynamic versus kinetic products. *J. Am. Chem. Soc.* **2015**,
        137 (25), 7947–7966.

62.   Huang, T.; Meng, F.; Qi, L., Controlled synthesis of dendritic gold
        nanostructures assisted by supramolecular complexes of surfactant with
        cyclodextrin. *Langmuir* **2009**, 26 (10), 7582–7589.

63.   Panda, B. R.; Chattopadhyay, A., Synthesis of Au Nanoparticles at "all" pH by
        H_2O_2 reduction of $HAuCl_4$. *J. Nanosci. Nanotechnol.* **2007**, 7 (6), 1911–1915.

64.   Pacławski, K.; Fitzner, K., Kinetics of reduction of gold (III) complexes using
        H_2O_2. *Metall. Mater. Trans. B* **2006**, 37 (5), 703–714.

65.   Pangeni, B.; Paudyal, H.; Abe, M.; Inoue, K.; Kawakita, H.; Ohto, K.; Adhikari,
        B. B.; Alam, S., Selective recovery of gold using some cross-linked
        polysaccharide gels. *Green Chem.* **2012**, 14 (7), 1917–1927.

66.   Parnklang, T.; Lertvachirapaiboon, C.; Pienpinijtham, P.; Wongravee, K.;
        Thammacharoen, C.; Ekgasit, S., H_2O_2-triggered shape transformation of silver
        nanospheres to nanoprisms with controllable longitudinal LSPR wavelengths.
        RSC Adv. **2013**, 3 (31), 12886–12894.

67. Parnklang, T.; Lamlua, B.; Gatemala, H.; Thammacharoen, C.; Kuimalee, S.; Lohwongwatana, B.; Ekgasit, S., Shape transformation of silver nanospheres to silver nanoplates induced by redox reaction of hydrogen peroxide. *Mater. Chem. Phys.* **2015**, 153, 127–134.

68. Gatemala, H.; Pienpinijtham, P.; Thammacharoen, C.; Ekgasit, S., Rapid fabrication of silver microplates under an oxidative etching environment consisting of O_2/Cl^-, NH_4OH/H_2O_2, and H_2O_2. *CrystEngComm* **2015**, 17 (29), 5530–5537.

69. Gatemala, H.; Thammacharoen, C.; Ekgasit, S., 3D AgCl microstructures selectively fabricated via Cl^--induced precipitation from $[Ag(NH_3)_2]^+$. *CrystEngComm* **2014**, 16 (29), 6688–6696.

70. Fievet, F.; Fievet-Vincent, F.; Lagier, J.-P.; Dumont, B.; Figlarz, M., Controlled nucleation and growth of micrometre-size copper particles prepared by the polyol process. *J. Mater. Chem.* **1993**, 3 (6), 627–632.

71. Ramaswamy, V.; Haynes, T. E.; White, C. W.; MoberlyChan, W. J.; Roorda, S.; Aziz, M. J., Synthesis of nearly monodisperse embedded nanoparticles by separating nucleation and growth in ion implantation. *Nano Lett.* **2005**, 5 (2), 373–377.

72. Zhuang, H.; Zhang, L.; Fuchs, R.; Staedler, T.; Jiang, X., When epitaxy meets plasma: a path to ordered nanosheets arrays. *Sci. Rep.* **2013**, 3, 2427.

73. Wang, Z.; Chen, Z.; Zhang, H.; Zhang, Z.; Wu, H.; Jin, M.; Wu, C.; Yang, D.; Yin, Y., Lattice-mismatch-induced twinning for seeded growth of anisotropic nanostructures. *ACS nano* **2015**, 9 (3), 3307–3313.

74. Qin, X.; Miao, Z.; Fang, Y.; Zhang, D.; Ma, J.; Zhang, L.; Chen, Q.; Shao, X., Preparation of dendritic nanostructures of silver and their characterization for electroreduction. *Langmuir* **2012**, 28 (11), 5218–5226.

75. Rai, A.; Singh, A.; Ahmad, A.; Sastry, M., Role of halide ions and temperature on the morphology of biologically synthesized gold nanotriangles. *Langmuir* **2006**, 22 (2), 736–741.

76. Shankar, S. S.; Bhargava, S.; Sastry, M., Synthesis of gold nanospheres and nanotriangles by the Turkevich approach. *J. Nanosci. Nanotechnol.* **2005**, 5 (10), 1721–1727.

77. Marinković, N. S.; Calvente, J. J.; Kloss, A.; Kováčová, Z.; Ronald Fawcett, W., SNIFTIRS studies of the electrochemical double layer: part II. Au (111) electrode in solutions with specifically adsorbed nitrate ions. *J. Electroanal. Chem.* **1999**, 467 (1–2), 325–334.

78. Moraes, I. R.; da Cunha, M. C. P.; Nart, F. C., Vibrational spectroscopy of adsorbed sulfate and nitrate ions on. *J. Braz. Chem. Soc.* **1996**, 7 (6), 453–460.

79. Li, Z. Y.; Xia, Y., Metal nanoparticles with gain toward single-molecule detection by surface-enhanced Raman scattering. *Nano Lett.* **2010**, 10 (1), 243–249.

80. Tian, N.; Zhou, Z. Y.; Sun, S. G.; Cui, L.; Ren, B.; Tian, Z. Q., Electrochemical preparation of platinum nanothorn assemblies with high surface enhanced Raman scattering activity. *Chem. Commun.* **2006**, (39), 4090–4092.

81. Mo, X.; Wu, Y.; Zhang, J.; Hang, T.; Li, M., Bioinspired multifunctional Au nanostructures with switchable adhesion. *Langmuir* **2015**, 31 (39), 10850–10858.

82. Joseph, V.; Matschulat, A.; Polte, J.; Rolf, S.; Emmerling, F.; Kneipp, J., SERS enhancement of gold nanospheres of defined size. *J. Raman Spectrosc.* **2011**, 42 (9), 1736–1742.

83. Zhang, Q.; Lu, X.; Tang, P.; Zhang, D.; Tian, J.; Zhong, L., Gold nanoparticle (AuNP)-based surface-enhanced Raman scattering (SERS) probe of leukemic lymphocytes. *Plasmonics* **2016**, 11 (5), 1361–1368.

84. Hildebrandt, P.; Stockburger, M., Surface-enhanced resonance Raman spectroscopy of Rhodamine 6G adsorbed on colloidal silver. *J. Phys. Chem.* **1984**, 88 (24), 5935–5944.

85. Huang, X.; Jain, P.; El-Sayed, I.; El-Sayed, M., Plasmonic photothermal therapy (PPTT) using gold nanoparticles. *Lasers Med. Sci.* **2008**, 23 (3), 217–228.

APPENDIX
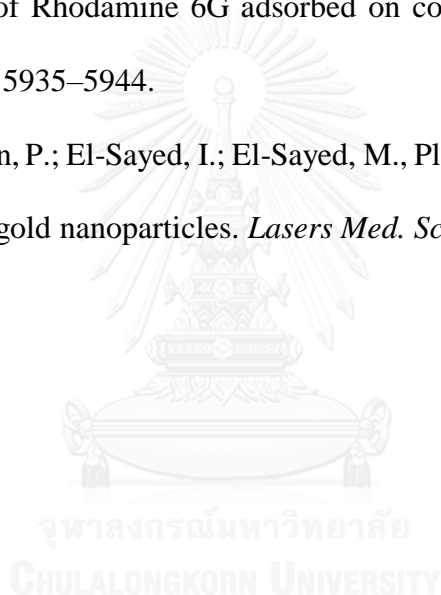
Research achievements

We have successfully developed the structural control synthesis of complex gold nanostructures (*i.e.,* QS-AuMSs, UL-AuMSs, HS-AuMSs and UL-AuNPs) using chemical approach and demonstrated their applications. These works were published in peer-review journals. We had participated in domestic and international conferences for presentation our work. Furthermore, our research works about engineering micro/nano structures of gold and silver were achieved many awards. The list of research achievements is shown below.

Research publications

1. Pangdam, A.; Nootchanat, S.; Ishikawa, R.; Shinbo, K.; Kato, K.; Kaneko, F.; Thammacharoen, C.; Ekgasit, S.; Baba, A., Effect of Urchin-Like Gold Nanoparticles in Organic Thin-Film Solar Cells. *Phys. Chem. Chem. Phys.* **2016**, 18, 18500–18506.

2. Nootchanat, S.; Pangdam, A.; Ishikawa, R.; Shinbo, K.; Kato, K.; Kaneko, F.; Thammacharoen, C.; Ekgasit, S.; Baba, A., Grating-coupled surface plasmon resonance enhanced organic photovoltaic devices induced by Blu-ray disc recordable and Blu-ray disc grating structures. *Nanoscale* **2017**, 9(15), 4963–4971.

3. Pangdam, A.; Wongravee, K.; Nootchanat, S.; Ekgasit, S., Urchin-like Gold Microstructures with Tunable Length of Nanothorns. *Mater. Des.* **2017**, 130, 140–148.

Awards

1. The outstanding poster award in Pure and Applied Chemistry International Conference 2010 (PACCON 2010), Thailand entitled "Investigation of self-assembled silver nanoparticles synthesized by green synthesis"

2. The Bangkok Bank Young Chemists award in 14th Asian Chemical Congress (14 ACC) 2011, Thailand entitled "Silver nanoparticles aggregation for colorimetric sensor and surface enhance Raman Spectroscopy"

3. The first prize of poster presentation award in The Science Forum 2012, Thailand entitled "Structure evolution of raspberry-like to urchin-like gold microstructures induced by silver ion"

4. The third prize in Sci&Tech Innovation and Sustainability Award: Innovative Chemical Processes & Produce 2012, Thailand entitled "Crystalline silver clay (CSC) for silver jewelry design and decorative"

5. The bronze medal in 40th International Exhibition of Inventions of Geneva 2012, Switzerland entitled "Crystalline silver clay"

6. The innovation award in 5th FAIR International Inventions and Innovation Exhibition 2013 (FINEX 2013), Iran entitled "Microcrystalline crystalline silver clay with low sintering temperature for silver jewelry designs and fabrications"

7. The excellence in science 2013 award by the Committee on Science, Technology, Communications and Telecommunications of the senate, Thailand entitled "Crystalline silver clay for silver jewelry design and creation"

8. NRCT invention awards 2013 by the National Research Council of Thailand, Thailand entitled "SHANNTA Silver Clay: The only Thai Brand Silver Clay for Design and Fabrication of Silver Jewelry"

Certificate

Certificate of Participation and Achievement 2013, entitled "Chemical Safety" from Chulalongkorn University and Center of Excellence on Hazardous Substance Management, Thailand

Conferences

1. Supeera Nootchanat, Apichat Pangdam, Prompong Pienpinijtham, Duangta Tongsakul, Chuchaat Thammacharoen, Sanong Ekgasit "Green synthesis of precious metals (Ag, Au, Pt, Pd) nanoparticles" (poster presentation) International conference of nanoscience & technology China (China Nano 2009), 1-3 September 2009, Beijing, China

2. Apichat Pangdam, Chuchaat Thammacharoen, Sanong Ekgasit "Investigation of self - assembled silver nanoparticles synthesized by green synthesis" (poster presentation) Pure and applied chemistry international conference 2010 (PACCON 2010), 21-23 January 2010, Ubon Ratchathani, Thailand

3. Apichat Pangdam, Chuchaat Thammacharoen, Sanong Ekgasit "Hydrogen peroxide determination via colorimetric sensor by silver nanoparticles aggregation" (oral presentation) The 36th congress on science and technology of Thailand, 26-28 October 2010, Bangkok, Thailand

4. Apichat Pangdam, Chutiparn Lertvachirapaiboon, Chuchaat Thammacharoen and Sanong Ekgasit "Silver nanoparticles aggregation for colorimetric sensor and surface enhance Raman Spectroscopy" (poster presentation) 14th Asian chemical congress (14 ACC), 5-8 September 2011, Bangkok, Thailand

5.   Apichat Pangdam, Chuchaat Thammacharoen, Sanong Ekgasit, "Structural evolution of raspberry- like to urchin - like gold microstructures induced by silver ion" (oral presentation) The 29thannual conference of the microscope society of Thailand (MST 29)30 January - 1 February 2012, Phetburi, Thailand

6.   Apichat Pangdam, Chuchaat Thammacharoen and Sanong Ekgasit "Structure evolution of raspberry - like to urchin - like gold microstructures induced by silver ion" (poster presentation) The science forum 2012, Faculty of Science, Chulalongkorn University,19-20 April2012, Bangkok, Thailand

7.   Apichat Pangdam, Chuchaat Thammacharoen and Sanong Ekgasit "Urchin-like gold micro/nanostructures (ULGMNSs) with exceptionally high SERS" (oral presentation) Pure and applied chemistry international conference 2014 (PACCON 2014), 8-10 January 2014, Khon Kaen, Thailand

8.   Apichat Pangdam, Chuchaat Thammacharoen and Sanong Ekgasit "Structure evolution of raspberry - like to urchin - like gold microstructures induced by silver ion" (poster presentation) The science forum 2012, Faculty of Science, Chulalongkorn University, 20-21 March 2014, Bangkok, Thailand

9.   Apichat Pangdam, Supeera Nootchanat, Kazunari Shinbo, Keizo Kato, Futao Kaneko, Ryousuke Ishikawa, Chutiparn Lertvachirapaiboon, Chuchaat Thammacharoen, Sanong Ekgasit and Akira Baba "Improved photovoltaic performance of organic thin-film solar cells (OSCs) with Urchin-like gold nanoparticles (UL-AuNPs)" (poster presentation) Polycondensation 2016, 11-15 September 2016, Moscow and St. Petersburg, Russia.

Scholarships

2005-2009   Human Resource Development in Science Project

                   (Science Achievement Scholarship of Thailand, SAST)

2009-2017   Research Assistant Scholarship

                   (Under Prof. Dr. Sanong Ekgasit, Chulalongkorn University)

2014-2017   The 90th anniversary of Chulalongkorn University Fund

                   (Ratchadaphiseksomphot Endowment Fund)

2015-2016   Overseas research experience scholarship for graduate student

                   (Graduate School, Faculty of Science and Department of

                   Chemistry, Faculty of Science, Chulalongkorn University)

2014-2017   "Global Circus" for double doctoral degree program,

                   Niigata University (Ministry of Education, Culture, Sports,

                   Science and Technology, Japan)

VITA

Name: Mr. Apichat Pangdam

Date of Birth: 14 December 1986

Address: 67/1 M.6, Sai Khueng, Phrasaeng, Surat Thani, 84210, Thailand

Mobile phone: +66-862-738712

E-mail: apichat.pangdam@gmail.com

Educations

2017 Ph. D. Chemistry

Chulalongkorn University, Bangkok, Thailand

2017 Ph. D. Electrical and Electronic Engineering

Niigata University, Niigata, Japan

2009 B. Sc. Chemistry

Prince of Songkla University, Songkhla, Thailand

Research interests

• Chemical synthesis and characterization of metal nanoparticles

• Nanoparticle stabilization and functionalization

• Localized surface plasmon resonance (LSPR) of metal nanoparticles

• Organic electronic device and plasmonic solar cells

• Surface enhanced Raman scattering (SERS) on metal nanostructures